Amyloids and Protein Aggregation–Analytical Methods

Huiyuan Li, Farid Rahimi, Sharmistha Sinha, Panchanan Maiti and Gal Bitan
University of California at Los Angeles, California, USA

Kazuma Murakami
Metropolitan Institute of Gerontology, Tokyo, Japan

More than 30 diseases are associated with amyloid-forming proteins, which undergo conformational alterations and "misfolding" under particular conditions. These proteins deposit as insoluble proteinaceous aggregates generating disease-specific histopathologic lesions. The proteins contributing to each disease have dissimilar sequences and native structures, yet they share the commonality of forming insoluble amyloid aggregates characterized by fibrillar morphology and cross-β structure. Presently, it is thought that the predominant agents causing cell toxicity and tissue damage are soluble, prefibrillar assemblies of these proteins. Because of the metastable nature of these prefibrillar assemblies and the noncrystalline nature of fibrillar protein aggregates, structural study of amyloid proteins is difficult. As a result, structural characterization of these proteins is typically done using combinations of low-resolution analytical methods. Here, we present a compendium of analytical methods used to study the secondary, tertiary, and quaternary structures, and morphology of prefibrillar and fibrillar assemblies of amyloid-forming proteins.

1 INTRODUCTION

Amyloid diseases are characterized by the deposition of insoluble aggregates and comprise over 30 diseases, including Alzheimer's disease (AD), Parkinson's disease (PD), Huntington's, and prion diseases, type-2 diabetes, senile systemic, atrial, and hereditary renal amyloidoses.[1,2] The amyloid deposits show characteristic Congo red (CR) binding, cross-β X-ray diffraction patterns, and straight, unbranched fibrillar morphology by electron microscopy.[3,4] Even though amyloid deposits have common structural characteristics, the contributing amyloid proteins have distinct primary structures.[4–6] At present, more than 24 different proteins or peptides are known to be associated with amyloid diseases.[7,8] In addition, work by Dobson and coworkers has shown that virtually any protein can be induced into forming amyloid, leading to the suggestion that amyloid is a primordial, highly stable polypeptide form, which had to be overcome by evolution to create functional globular proteins.[9] Interestingly, when compared directly, fibrils formed by proteins not associated with disease did not show cellular toxicity, whereas prefibrillar assemblies of

the same proteins were toxic.[10] Thus, there is considerable interest in studying the structures and assembly mechanisms of proteins into amyloid structures and their precursors.

The proteins that cause amyloid-associated diseases can be divided into two classes based on their native structures – globular proteins and natively unfolded proteins. For the first group, which includes, e.g. prion, transthyretin (TTR), Cu/Zn superoxide dismutase 1, and β_2-microglobulin (β2m), amyloid formation appears to require a step of partial unfolding, leading to an unstable intermediate(s) that self-associates into β-sheet-rich toxic aggregates. Proteins in the second group, including amyloid β-protein (Aβ), α-synuclein, and tau presumably undergo partial folding creating a similar unstable intermediate that undergoes conformational transformation into a β-sheet-rich structure and self-assembly.[11]

Historically, amyloid has been defined as extracellular deposition of proteinaceous material composed of fibrils.[12] In many cases, protein aggregates accumulate intracellularly, producing structures that are similar in every way to amyloid but formally are called *amyloidlike*, merely because they are intracellular.

Common methods used for studying the formation and structural characteristics of amyloid proteins are listed in Table 1 and categorized according to the assembly state under study and the features investigated. Though we tried to be inclusive, we could not, and had no intention to encompass every method ever used to study amyloid proteins, but rather to cover the most commonly used methods. We discuss nuclear magnetic resonance (NMR), X-ray crystallography, and X-ray absorption – techniques that are used to resolve protein structure at the atomic level; lower resolution methods, including X-ray fiber diffraction and neutron scattering; spectroscopic methods, including circular dichroism (CD), Fourier transform infrared spectroscopy (FTIR); tinctorial methods such as CR binding, and changes in fluorescence of thioflavin dyes, which are used to characterize secondary structures; microscopic techniques including, transmission electron microscopy (TEM), scanning transmission electron microscopy (STEM), scanning tunneling microscopy (STM), and atomic force microscopy (AFM) that examine the morphology of prefibrillar and fibrillar protein assemblies; electron spin resonance (ESR), hydrogen–deuterium (H/D) exchange, limited proteolysis, and intrinsic fluorescence, which are applied to characterize tertiary and quaternary structures; and finally, methods used to study assembly size distribution, including gel electrophoresis, cross-linking, size-exclusion chromatography (SEC), analytical ultracentrifugation (AUC), dynamic light scattering (DLS), and ion-mobility spectrometry–mass spectrometry (IMS–MS). We survey the principles of the methods, instrumentation, experimentation, and their application in the amyloid field.

Table 1 Analytical methods used to study amyloid protein structure, folding, and assembly

	Monomer	Oligomer	Protofibril	Fibril	Amyloid (in vivo)
Atomic structure	Solution-state NMR			Solid-state NMR	
				X-Ray crystallography	
	X-Ray absorption				
Secondary structure	Circular dichroism spectroscopy				
	Fourier transform infrared spectroscopy				
			X-Ray fiber diffraction		
			Neutron scattering		
				Congo red binding / Thioflavin S fluorescence	
				Birefringence	
			Thioflavin T fluorescence		PIB/FDDNP/SB13/BF227
Morphology		Transmission electron microscopy			
		Scanning transmission electron microscopy			
		Scanning tunneling microscopy			
		Atomic force microscopy			
Tertiary/quaternary structure	Electron spin resonance				
	Hydrogen–Deuterium exchange				
	Limited proteolysis				
	Fluorescence methodologies				
Assembly size/size distribution	Gel electrophoresis				
	PICUP				
	Size-exclusion chromatography				
	Analytical ultracentrifugation				
	Dynamic light scattering				
	IMS–MS				

2 ATOMIC STRUCTURE

Two experimental methods enable determination of three-dimensional (3D) structures of proteins and protein complexes at atomic resolution – NMR spectroscopy and X-ray crystallography.[13] These methods are of limited use in the amyloid field, though recent advances in studies of soluble monomers and oligomers and of insoluble fibrils are encouraging.

2.1 Nuclear Magnetic Resonance Spectroscopy

Structure determination by NMR is based on the magnetic properties of the nuclei in the atoms comprising a molecule, or a macromolecular assembly under study. NMR occurs when nuclei with nonzero spin quantum numbers are placed in a powerful magnetic field and subjected to radiofrequency irradiation. The most informative nuclei are those with magnetic spin of 1/2. In biological material, these include ^{1}H, ^{13}C, ^{15}N, ^{19}F, and ^{31}P. The resonance signals and their characteristics, e.g. chemical shift, linewidth, J-coupling, cross-peaks, and nuclear Overhauser effect (NOE), are correlated to the nuclear environment and can be used for determining the 3D structures. The mechanisms, parameters, instrumentation, protein structure calculation by NMR techniques were introduced in detail elsewhere (*see* **Nuclear Magnetic Resonance of Biomolecules**; **Solution Nuclear Magnetic Resonance: Spin-1/2 Nuclei Other than Carbon and Proton**; **Multidimensional Nuclear Magnetic Resonance of Biomolecules**; **Nuclear Magnetic Resonance Instrumentation**; **Parameters, Calculation of Nuclear Magnetic Resonance**).

Solution-state NMR and solid-state NMR (ssNMR) are two branches of NMR spectroscopy that differ substantially in sample preparation, instrumentation, parameters, and the type of structural information extracted. These methods have been applied in different areas of studying amyloids and protein aggregation.

2.1.1 Solution-State Nuclear Magnetic Resonance

Solution-state NMR is a powerful high-resolution method for studying 3D structures of soluble samples. The most commonly used nuclei in solution-state NMR studies of protein structure are ^{1}H, ^{13}C, and ^{15}N. Resonances of these nuclei and interactions among them often can resolve all or most of the individual amino acids in small proteins ($\leq$60 kDa). Because peptides and proteins are relatively large molecules comprising repeating units (amino acids), signals in one-dimensional (1D) NMR spectra overlap substantially and the spectra typically cannot be interpreted without additional information. The information can be deconvoluted by the introduction of additional spectral dimensions, which correlate two different experimental parameters, thereby creating more unique signatures for each amino acid in the sequence. Many types of multidimensional NMR are used in structural studies of peptides and proteins (*see* **Multidimensional Nuclear Magnetic Resonance of Biomolecules**). These include both correlations between two different features of the same type of nucleus (homonuclear multidimensional NMR) or among different nuclei (heteronuclear multidimensional NMR).

Solution-state NMR is useful for studying amyloidogenic peptide and protein monomers, but when the monomers aggregate into oligomers, the signals become broad and eventually disappear due to the increase in tumbling time.[14] Changes in spectroscopic features, such as chemical shift, linewidth, cross-peaks, and NOE thus can be used to monitor the transition from monomer to oligomers[14,15] (for example, see Figure 1[16]). The cross-peaks displayed by two-dimensional (2D) NMR are used to identify the folding of a protein, including the secondary structures and long-range interactions among different regions.[17–19] NOE signal intensity, J-coupling constants, and chemical shift data are useful for calculating distances and torsion angles of correlated atoms.[19,20]

The heterogeneous nature of amyloidogenic protein oligomers and the high concentrations needed for NMR experiments add to the difficulty of studying such oligomers by solution-state NMR.[21] Early studies of Aβ, TTR and α-synuclein have been performed using fragments rather than the full-length protein, at
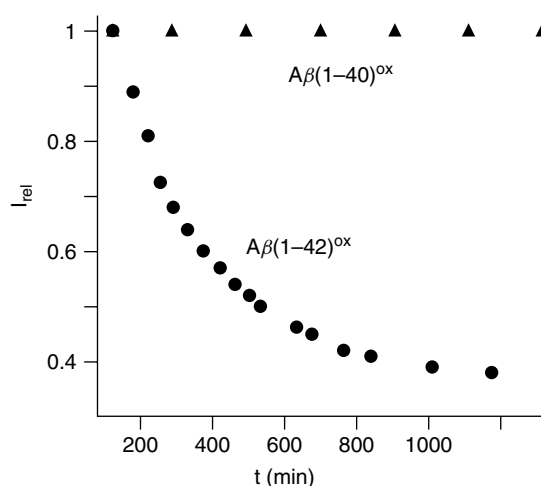
Figure 1 Aggregation behavior of Aβ(1–40)^{ox} and Aβ(1–42)^{ox}.[16] The sum of the signal volumes with chemical shifts between 0.0 and 1.5 ppm in the 1D ^{1}H NMR spectra of freshly prepared aqueous solutions of Aβ(1–40)^{ox} and Aβ(1–42)^{ox} is plotted vs the time that has elapsed after the sample preparation. (Reproduced from Ref. 16. © Blackwell Publishing Ltd, 2001.)
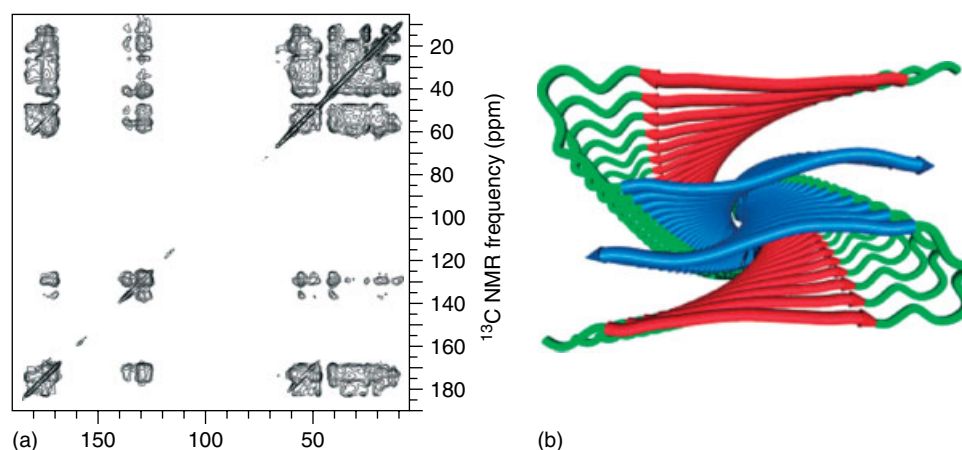
Figure 2 2D ssNMR spectrum and structure model for Aβ40 fibrils.[39] (a) 2D ss ^{13}C–^{13}C NMR spectrum of Aβ40 fibrils (^{15}N, ^{13}C-labeled at residues K16, F19, A21, E22, I32, and V36), recorded at 14.1 T with a 500-ms mixing period and 18.0-kHz MAS frequency. (b) Structural models for Aβ40 fibrils with F19/L34 internal quaternary contacts. Models were generated by a restrained molecular dynamics and restrained energy minimization protocol, applied to a dodecameric cluster of Aβ$_{9-40}$ molecules, with all restraints being derived from ssNMR measurements. Residues 1–8 are disordered, and were omitted from the modeling calculations. (Reproduced from Ref. 39. © American Chemical Society, 2006.)

nonphysiologic pH, and/or in mixtures of water and fluorinated alcohols or detergents to increase the solubility, disrupt quaternary structures, and dissociate peptide aggregates.[22–25] Though these studies were technically sound, their relevance to physiologic conditions was difficult to assess. Later studies developed techniques for studying full-length amyloidogenic peptides and proteins in dilute aqueous solutions. For example, full-length Aβ was studied with solution-state NMR in aqueous solution at neutral pH.[26,27]

2.1.2 Solid-State Nuclear Magnetic Resonance

ssNMR is typically used in studies of insoluble and noncrystalline solid-state molecular systems that are not suitable for solution-state NMR or X-ray crystallography (*see* **Solid-state Nuclear Magnetic Resonance**). ssNMR is the main tool available, to date, for obtaining high-resolution structural information of amyloid fibrils. The absence of isotropic tumbling in solid-state samples implies that dipole–dipole couplings and chemical shift anisotropies are not averaged. As a result, linewidth in ssNMR spectra are broadened relative to solution-state NMR, resulting in lower resolution. On the other hand, the absence of tumbling enables studying effects of anisotropic or orientation-dependent interactions. Cross polarization (CP), high-power proton decoupling, and magic-angle spinning (MAS) are used as standard techniques to obtain high-resolution ssNMR spectra. The isotropic chemical shift values obtained from CP–MAS experiments can be used to determine site-specific secondary structures.

In recent years, ssNMR has allowed for substantial advancement in understanding the structure of amyloid fibrils. In fibrillar samples, CP–MAS is useful for observing rigid fibrillar parts, whereas dipolar-dephasing MAS is used to detect soluble components of mobile parts.[28,29] Rational resonance is used for determining homonuclear–internuclear distances, and rational-echo double-resonance is used to determine heteronuclear–internuclear distances.[30,31] Other techniques, such as radio-frequency-driven recoupling and dipolar-assisted rational resonance, are useful for obtaining folding information of amyloid fibrils.[32]

The ssNMR studies of full-length Aβ, Aβ fragments including Aβ(34–42), Aβ(10–35), transthyretin (TTR$_{105-115}$), α-synuclein, prion protein fragments HET-s$_{218-289,}$ and PrP$_{89-143}$, and the dialysis-related amyloidosis protein β$_2$-microglobulin (β2m) are discussed in recent review articles.[33–38] Figure 2 shows an example of 2D ^{13}C–^{13}C ssNMR correlation spectra of Aβ40 fibrils with uniform ^{15}N and ^{13}C labeling at specific residues and a structural model of Aβ40 fibrils that was generated based on ssNMR measurements.[39]

2.2 X-Ray Crystallography

X-ray crystallography examines atomic structures of crystals using diffraction patterns of X-ray radiation directed at homogeneous single crystals in which molecules exist in highly ordered repetitive units (*see* **X-ray Techniques: Overview**; **Structure Determination, X-ray Diffraction for**). The repetitive patterns, or "unit cells", within a crystal amplify the diffraction signals, which are collected and converted into 3D electron-density maps. The positions of the atom nuclei are

deduced from the electron-density maps. On the basis of these data and complementary chemical information, 3D models of the molecules or macromolecular assemblies in the crystal are obtained.

For details about mechanism and instrumentation of X-ray crystallography (see **X-ray Crystallography of Biological Macromolecules**). The critical step for X-ray crystallography is obtaining a crystal with high diffraction quality. This is often difficult to achieve due to high structural freedom of macromolecules. Gradually lowering the solubility of the molecule of interest in an appropriate solution is a common approach for obtaining high-quality crystals.[40] Fibrils formed by amyloidogenic peptides and proteins are highly ordered structures, yet their degree of order is not high enough to produce high-resolution diffraction patterns as the way single crystals do. Fiber and powder X-ray diffraction methods do not require single crystals and have been applied widely for determination of secondary structures of amyloid protein fibrils (see Section 3.2.1).

X-ray crystallography has been used for determining the structures of amyloidogenic proteins that natively form a stable fold, i.e. in their nonamyloid form. For example, the crystal structures of bovine β2m, wild-type human β2m, and mutant human H31Y-β2m have been reported.[41] Seven-stranded β-sandwich folds were observed in crystal structure of the monomeric form of wild-type human β2m.[42] The crystal structures of human cystatin C (HCC), which are associated with hereditary cystatin C amyloid angiopathy, reveal that a full-length HCC dimer with swapped domains is present in an asymmetric unit of a tetragonal crystal.[43–45] Crystallographic structures of several TTR variants and of prion proteins also have been solved.[46–48] Using X-ray microcrystallography techniques, the structures of 30 short (6–7 residues) segments of amyloidogenic proteins, including Aβ, tau, PrP, insulin, islet amyloid polypeptide (IAPP), lysozyme, myoglobin, α-synuclein, and β2m recently have been determined and, in multiple cases, were found to be organized in a "steric zipper".[49,50]

In particular cases, amyloidogenic peptides fused to a larger protein,[51] small molecules,[52] or co-crystallized as antigen–antibody complexes[53,54] can yield high-resolution structures. For example, the crystal structure of the fragment Aβ(28–42) fused with the C-terminal region of ribonuclease HII from *Thermococcus kodakaraensis* was determined by Takano et al.[51] In this fusion protein, Aβ(28–42) formed a β-hairpin conformation centered around a turn at V36–V37. A fragment of the monoclonal antibody WO2, which recognizes the N-terminal region of Aβ, was complexed with Aβ(1–16) or Aβ(1–28) and produced homogeneous crystals suitable for X-ray crystallographic studies.[53,54] In these complexes, Aβ peptide adopted an extended, coiled conformation in the major immunodominant B-cell epitope between residues 2–8.

2.3 X-Ray Absorption Spectroscopy

X-ray absorption spectroscopy (XAS) is a technique that provides information on the local environment and electronic state around heavy atoms in biomolecules (see **Absorption Techniques in X-ray Spectrometry**). When a high-energy X-ray beam hits a sample, certain energy is absorbed and electrons are excited and ejected from their orbitals (photoelectrons). The energy absorption occurs at defined energy levels corresponding to the binding energy of the electrons in the heavy atom. When a photoelectron leaves the absorbing atom, its wave is backscattered by the neighboring atoms. The XAS is the plot of absorption coefficients of heavy atom against the incident X-ray energy.

XAS spectra typically are divided into two regions designated X-ray absorption near-edge structure (XANES) and extended X-ray absorption fine structure (EXAFS). XANES is restricted up to 50 eV. EXAFS extends up to 1000 eV above the threshold energy. In the XANES region, transitions of core electrons to nonbound levels with close energy occur. In the EXAFS region, the photoelectrons have high kinetic energy and single scattering by the nearest neighboring atoms normally dominates (see **Absorption Techniques in X-ray Spectrometry**).

Because EXAFS has chemical selectivity and sensitivity to the local atomic arrangement around the absorbing (heavy) atom, it is particularly useful for studying amino acid residues coordinating metal ions.[55–57] The pathologies of several amyloid diseases (such as AD, PD, and prion diseases) may involve interaction of the *culprit* amyloid protein associated with each disease (Aβ, α-synuclein, and PrP, respectively) with metal ions, such as Cu^{2+}, Zn^{2+}, and Fe^{3+}.[58] Atomic information about metal-binding amyloid-peptide models and metal-binding sites are useful in understanding the function of transition metals in peptide aggregation and redox chemistry in these diseases.[56,58] In AD, a major cause of neurotoxicity is reactive oxygen species whose production in the brain may involve Aβ-complexed Cu ions.[59] Stellato et al. reported EXAFS studies of Aβ40–Cu^{2+} complexes and suggested that Cu^{2+} is penta-coordinated to three nitrogen atoms of three histidines (His6, His13, and His14) and two oxygen atoms, one belonging to Tyr (Tyr10) and the other, from either a water molecule or an acidic residue.[57] A number of studies have linked cellular prion function to its ability to bind Cu^{2+}, playing a role in the copper uptake from extracellular environment to endosomes and the inverse release process.[60,61] EXAFS experiments suggested that

a square planar four-nitrogen–Cu^{2+} coordination is formed in prion–Cu^{2+} complexes,[62,63] in which two nitrogen atoms are contributed by imidazole rings of histidine residues and the other two nitrogen atoms are deprotonated backbone atoms.

3 SECONDARY STRUCTURE

3.1 Secondary Structure – Spectroscopic Methods

Spectroscopic methods are used widely for structural characterization and biophysical analyses of various assemblies of amyloid proteins. Typically, spectroscopic techniques are used to study these proteins in vitro, under conditions that are simpler than the in vivo environments, allowing delineation of fine details and specific interactions. Spectroscopic techniques can be used to obtain a unique signature, allowing detection and identification of specific amyloid proteins or particular structures that are common to these proteins, or to decipher the actual structure of a region within a protein or a protein assembly. Here, we discuss CD and FTIR for studying secondary structure of amyloid proteins.

3.1.1 Circular Dichroism Spectroscopy

CD spectroscopy (see **Circular Dichroism in Analysis of Biomolecules**; **Circular Dichroism and Linear Dichroism**) measures differential absorption of circularly polarized light by chiral centers as a function of wavelength. Far ultraviolet (UV) CD spectra (180–250 nm) of peptides and proteins are highly sensitive to secondary structures due to the effect of the dihedral angle of peptide bonds on the absorption of the chiral center at the α-carbon. In contrast, near-UV CD spectra (250–350 nm) reflect contributions of aromatic side chains and disulfide bonds, and provide information about polypeptide tertiary structure.[64]

Samples for CD spectroscopy are typically dissolved in aqueous buffers with or without co-solvents. The choice of buffers and co-solvents is critical. Most of the structural information of proteins is obtained in the far-UV range. Several chemical bonds have strong absorption in this region. Hence, buffers should be chosen such that they have minimal absorption in this region. A typical buffer used in CD experiments is 10 mM phosphate.[64]

CD is an averaging technique, which provides information about the conformational state of an entire ensemble of molecules in a given sample. Quantitative assessment of secondary structures can be achieved by deconvolution of experimental spectra using libraries of existing known structures.[65] Nevertheless, on the basis of CD data alone, it is impossible to distinguish, for example, between a situation in which part of a protein monomer is α-helical and another in β-sheet conformation, and a heterogeneous population in which a percentage of the monomers are purely helical and the other part is entirely in a β-sheet conformation.

Aggregation of amyloidogenic proteins into protofibrils (short, curvilinear fibril precursors[66,67]) and fibrils is accompanied by abundant formation of β-sheet conformation. This phenomenon can be detected by the characteristic appearance of an absorption minimum at 215–218 nm in the far–UV CD spectrum. CD is typically used for qualitative determination of the nature of amyloid assemblies and kinetics of conformational transitions associated with aggregation. Fine details, such as the orientation of monomers with β-sheets (parallel or antiparallel) cannot be determined on the basis of CD data. An advantage of CD relative to other methods for determination of secondary structure is its tolerance of a wide range of pH and temperature. For example, low pH compromises the binding of dyes such as CR and thioflavin T to amyloid samples (see Section 3.3) making detection of β-sheet formation by these dyes at acidic pH difficult.

The understanding of mechanistic pathways of amyloid formation for multiple proteins has been facilitated by CD. For example, studies of prion proteins have shown that a conformation composed predominantly of α-helical and ''random-coil'' secondary structures eventually transforms into β-sheet-rich conformations in an NaCl solution, whereas, a soluble β-sheet-containing form of the protein generated in the presence of 0.03 % sodium dodecyl sulfate (SDS) leads to formation of a structure that is predominantly random coil.[68] (The term ''random coil'' is a common name for irregular conformations characterized by a maximum at 212 nm and a minimum at 196 nm in the CD spectrum. It points to the fact that the conformation is distinct from common secondary structure elements, such as α-helix, β-sheet, or β-turn, but does not suggest that the conformation indeed is random.) The presence of α-helical and/or partially unfolded intermediates on the pathway of amyloid formation has been demonstrated for other amyloidogenic proteins. Kirkitadze et al. have shown that formation of a partially helical intermediate is a general feature of Aβ fibrillogenesis and that helix content and the kinetics of helix formation were affected by amino acid substitutions that cause familial AD.[69] The rate of helix formation was found to correlate with changes in the ionization state of His and Asp residues.

Taking advantage of the tolerance of CD to a wide range of pH, it has been demonstrated that the N-terminal fragment (residues 1–29) of horse heart apomyoglobin was highly prone to aggregation accompanied by β-sheet formation at low pH (pH 2.0) but not at pH 8.3.[70,71] In

another example, it has been demonstrated that for ABri, a 34-residue peptide that causes British dementia, there is a substantial loss of random coil structure as the pH of the system is raised from acidic to neutral and then to basic.[72]

3.1.2 Fourier Transform Infrared Spectroscopy

IR spectroscopy (*see* **Fourier Transform Infrared Spectroscopy in Peptide and Protein Analysis**; **Infrared Spectroscopy: Introduction**; **Infrared Spectroscopy of Biological Applications**; **Infrared Spectroscopy in Clinical Chemistry**) is complementary to CD for studying secondary structure of proteins capable of providing quantitative information about secondary structural elements.

A strong absorption band at $\sim$1600–1700 cm^{-1} in IR spectra of proteins has been assigned to the vibration of C=O bonds in the polypeptide main chain. This spectral feature is particularly sensitive to, and therefore serves as an informative proxy for, secondary structural elements. This region is called the amide-I region. Similarly, C–N stretching and N–H bending vibrations give rise to absorption bands at 1550 cm^{-1} (amide-II) and 1250 cm^{-1} (amide-III) and are useful for assignment of secondary structure. Following deconvolution of the amide-I band contour, secondary structure content is estimated by taking into account the relationship between peak position and the type of secondary structures. IR absorption intensity is proportional to $\left(\frac{\delta\mu}{\delta qi}\right)^2$ where μ indicates dipole moment of a molecule and qi denotes the ith normal coordinate. Oscillation of charged groups results in displacement of charges that in turn bring about larger value of $\left(\frac{\delta\mu}{\delta qi}\right)^2$, thus resulting in larger absorption.

The main bands of interest in the amide-I region for the detection of amyloidogenic protein regions in fibrils are at 1626 and 1632 cm^{-1} for parallel β-sheet structure and at 1690 cm^{-1} for antiparallel β-sheet. The signature of random coil (extended, irregular structure with distinct spectroscopic features) is a band at 1644 cm^{-1} and that of α-helix is a band at 1654 cm^{-1}. However, α-helical conformations also contribute to band intensities at 1644 and 1662 cm^{-1}, making distinction from random coil difficult. Non-α and non-β structures appear at <1660 cm^{-1}. Although strong signals corresponding to particular secondary structures exist in this region, information in IR spectra obtained in aqueous buffers is masked by a strong signal at 1630 cm^{-1} due to water bending vibrations. Hence, alternative strategies have been adopted to probe the secondary structure of proteins in general, and amyloidogenic proteins in particular, with IR spectroscopy.

Isotopic substitution has far-reaching effects on IR absorption. The peak positions of ^{13}C=O and C=O^{18} stretching bands shift to lower frequency relative to ^{12}C=O^{16} bands. Isotopic labeling thus allows assignment of secondary structures at a single-residue level. For example, for α-helix, the ^{13}C=O appears at 1600 cm^{-1}, whereas ^{13}C=O β-sheet bands are at 1586 cm^{-1} (parallel) and 1595 cm^{-1} (antiparallel). Another isotopic labeling strategy is changing the solvent from H$_2$O to D$_2$O. This shifts the water bending vibration peak from 1630 to 1290 cm^{-1} facilitating measurement in the amide-I region.

Attenuated total-internal reflection Fourier transform infrared (ATR-FTIR) spectroscopy is a powerful method for recording IR spectra of biological samples.[73,74] Typically, ATR-FTIR studies are performed with the sample applied on a trapezoidal germanium plate. The IR beam is aimed at a high-refractive-index medium (transparent to the IR radiation of interest, e.g. germanium or diamond). If the incident beam is above the critical angle of refraction (the critical angle depends on the ratio of the refractive indexes of the plate and the external medium), the light beam is reflected completely when hitting the surface of the plate. Several internal reflections occur within the plate when the light reaches the other end. Samples deposited on the surface of the plate absorb electromagnetic radiation of an evanescent wave, thereby reducing the intensity of the reflected light, which is collected eventually at the detector (see Figure 3). Sample preparation for ATR-FTIR involves spreading a drop (5–50 μL) on a germanium or diamond plate and slow evaporation of the solvent, typically under a stream of dry nitrogen gas. This enables minimal contribution from the solvent in the spectra. The main advantage of ATR-FTIR compared to the traditional FTIR is that the signal gets amplified many times. In the traditional FTIR, the sample and the IR light interact only once. However, in ATR-FTIR due to the repeated reflections of the incident beam on the trapezoid plate, the sample has more chance to absorb the incident IR light resulting in greater absorption. This leads to high signal-to-noise ratio. Further, the background due to the solvent is also minimized.
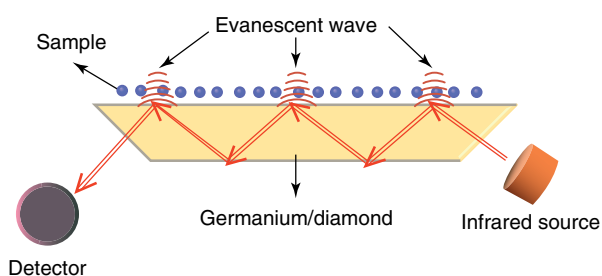

Figure 3 Schematic representation of instrumentation in ATR-FTIR.

The mechanism of aggregation for a number of amyloidogenic proteins has been probed by ATR-FTIR. For example, using this technique, Fink and coworkers have demonstrated formation of a dominant helical structure which finally transforms to a structure rich in β-sheet during aggregation of insulin.[75] ATR-FTIR also has been used to show that the extent of β-sheet in β2m amyloid fibrils made in vitro was similar to those taken from patients with dialysis-related amyloidosis.[76]

Linear dichroism IR is a spectroscopic method that yields detailed information about objects in highly ordered arrays. Linear dichroism measures differential absorption of parallel and perpendicular light directions. Combining the dichroism and absorption measurements, the orientation of particular functional groups with respect to the alignment axis can be deduced. These studies enable deciphering the nature of β-sheets, e.g. detecting twisted or bent sheets in an array by noting positive and negative features in the parallel and perpendicular directions of the transition dipole moments with respect to the alignment axis.[77] Linear dichroism infrared spectroscopy of Aβ(21–31) suggests that the β-sheet consists of two parts, which are twisted or bent relative to each other at an angle of 32°.[78]

Two-dimensional IR (2DIR) correlation spectroscopy is useful for determining protein structure and orientation. Detailed information regarding the arrangement of antiparallel β-sheet of different proteins such as lysozyme, ribonuclease A, concanavalin A, and poly-L-lysine has been obtained using this technique.[79] 2DIR spectra spread the vibrational resonances over two frequency dimensions, revealing couplings between

vibrations through the formation of cross-peaks in the spectrum, similar to the principle of 2D NMR. Recently, Hochstrasser and coworkers have observed linear chain excitation of amide units with isotopic labeling of Ala21, Gly29, Gly33, and Gly38 in Aβ40 fibrils.[80] Excitation was not observed for isotopically labeled Gly25, suggesting rigidity of the residues at positions 21, 29, 33, and 38 and flexibility at position 25 in Aβ40 fibrils. Zanni and coworkers have modified the method of obtaining 2DIR spectra developed by the Hochstrasser group using pulses with different times and frequencies that reduce spectral distortion and improve signal-to-noise ratio. Applying this method in kinetic studies of human IAPP aggregation, the authors showed that monitoring at 1618 and 1644 cm^{-1} in separate dimensions permitted monitoring random-coil and β-sheet populations without deconvolution.[81]

3.2 Secondary Structure – Diffraction and Scattering Methods

3.2.1 X-Ray Fiber Diffraction

In contrast to X-ray crystallography, which requires high-quality single crystals, X-ray fiber diffraction (*see* **Structure Determination, X-ray Diffraction for**) is executed on pulverized or lower quality crystalline samples and is used to gather information on the preferred orientation of the molecules in these samples. The X-ray diffraction patterns of almost all amyloid fibers exhibit broad equatorial reflections at ~10 Å and meridional reflections at ~5 Å.[82] This is a characteristic of a β-sheet structure in which the β-strands are arranged perpendicular to the fibril axis (cross-β arrangement). The X-ray diffraction pattern of human IAPP exhibits meridional

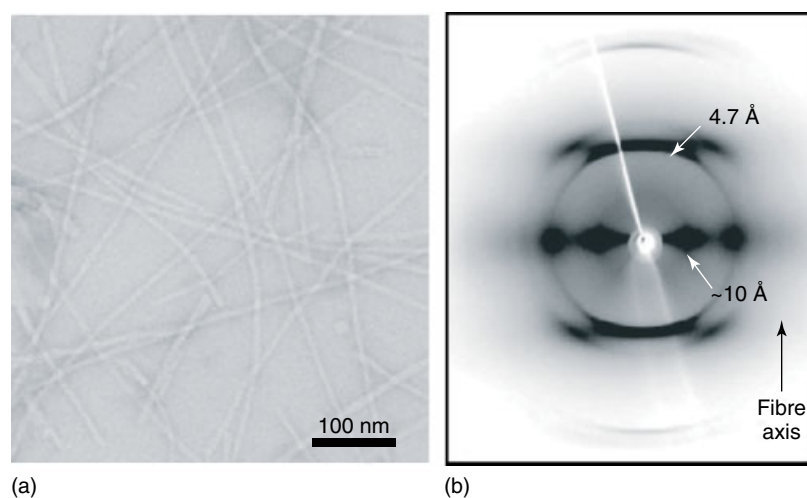(a)   (b)

Figure 4 The characteristics of amyloid fibrils include their appearance in the electron microscope and the cross-β diffraction pattern.[4] (a) Electron microscopy (EM) of negatively stained amyloid fibrils formed by IAPP showing long, unbranched fibrils of ~100 Å in diameter. (b) X-ray fiber diffraction pattern from magnetically aligned IAPP amyloid fibrils, showing the positions of the 4.7 Å meridional and ~10 Å equatorial reflections in a cross-β pattern. (Reproduced from Ref. 4. © Blackwell Publishing Ltd.)

reflections at ~4.7 Å and equatorial reflections at 10–11 Å (see Figure 4).[4] Highly oriented diffraction patterns with layer line spacing of ~9 Å represent antiparallel β-sheet structure.[83] These reflections vary depending on the side-chain composition of the aggregating peptide or protein. For example, scrapie prion fibrils give 4.72 Å meridional and 8.82 Å equatorial reflections.[84] The meridional reflections provide an estimate of the number of protofilaments comprising the fibril, whereas the equatorial reflections correspond to the spacing between the protofilaments. X-ray fiber diffraction patterns of amyloid fibers formed from six different proteins show a similar structure of helical arrangement of β-sheets parallel to the fiber long axis, with the strands perpendicular to this axis. The helical repeat is shown to be 115.5 Å and each repeat consists of 24 β-strands.[82]

3.2.2 Neutron Scattering

Neutron scattering (*see* **Neutron Scattering in Analysis of Polymers and Rubbers**) is used, often in combination with X-ray diffraction techniques, to study the structure of amyloid fibers. X-rays are scattered by the electrons surrounding atom nuclei, whereas neutrons are scattered by the nuclei themselves. This has several important consequences. For example, neutrons can be used to detect protons, which cannot be detected by X-rays. This helps assigning hydrogen-bond patterns in 3D structures of macromolecules and investigating strand orientation (parallel or antiparallel) in amyloid fibrils. Small-angle neutron scattering (SANS) provides information about size, shape, and extent of aggregation of the species under consideration and measurement of mass per unit length.[85] $A\beta40$ protofibrils have been found by SANS to be cylindrical structures with 24 Å cross-sectional radii and ~110 Å length.[86] Each cylindrical unit was reported to comprise 30 $A\beta40$ monomers. Another SANS study has shown that at neutral pH, $A\beta(10–35)$ self-assembles into supercoiled long nanotubes with an inner diameter of 44 and 4-nm-thick walls.[87] SANS investigation of the aggregation of α-chymotrypsin in the presence of a photo-responsive surfactant has shown that under visible light, extended hexameric structures are formed. Upon UV illumination, these hexamers combined into dodecamers similar to amyloid protofilaments.[88]

3.3 Secondary Structure – Tinctorial Methods

Detection of amyloid by staining is a practice more than a century old. In 1854, Rudolph Virchow introduced the term amyloid (starchlike, from the Latin word *amylum*) to denote a macroscopic tissue abnormality that exhibited a positive iodine-staining reaction.[89] The most conventional way of detecting amyloids for almost a century has been staining methods such as CR or thioflavin-type dyes (Figure 5).

3.3.1 Congo Red Binding and Birefringence

CR staining is commonly used for the identification of amyloid in tissue sections.[91,92] CR has two features enabling detection of amyloid. First, its alkaline solution stains amyloid with an intense red color resulting from a shift in the wavelength of maximal absorption from 490 to 540 nm upon binding to amyloid samples. This characteristic enables spectroscopic detection of amyloid and measurement of fibril formation. Second, upon binding to amyloid, CR yields a unique blue–green birefringence under cross-polarized light enabling visual determination of amyloid formation. This phenomenon was observed first by the Belgian physician Paul Divry in 1927 while studying degeneration of aging brain[93] and is still used, to date, to detect amyloid in tissue sections (Figure 5e).[90] The mechanism of CR binding to amyloid fibrils is not understood. Putative mechanisms are shown in Figure 5(d). One hypothesis is that the dye intercalates in between β-strands parallel to the peptide chains and perpendicular to the fibril direction.[94] Alternatively, binding may occur through interaction between the dye's negatively charged sulfonate groups with the positive N-termini of polypeptides such that the dye's axis is perpendicular to the length of the peptide and parallel to the direction of fibril axis.[95,96]

For a successful birefringence assay, the tissue thickness should be 5–10 μm. In addition, high salt concentrations and alkaline pH are required for binding and birefringence.[97]

3.3.2 Thioflavin T and Thioflavin S Fluorescence

The structure of Thioflavin T (ThT) has both polar and nonpolar functional groups (Figure 5a), leading to formation of micelles in aqueous solutions with the nonpolar dimethylaminophenyl groups in the core and the charged benzothiazole groups exposed to the solvent. ThT micelles bind to β-sheet structures resulting in intensified fluorescence signals relative to unbound ThT.[98] Vassar and Culling first introduced the use of this dye in 1959 for detecting amyloid tissue in kidney.[99] In the unbound state, excitation and emission occur at 342 and 430 nm respectively, whereas upon binding to amyloid samples, the excitation and emission of ThT undergo a bathochromic shift to 444 and 482 nm, respectively.[100] ThT has been employed mostly to characterize amyloid aggregates in vitro and ex vivo, whereas uncharged thioflavin derivatives have been used to detect amyloid in vivo.[101] Apart from the regular spectral measurements
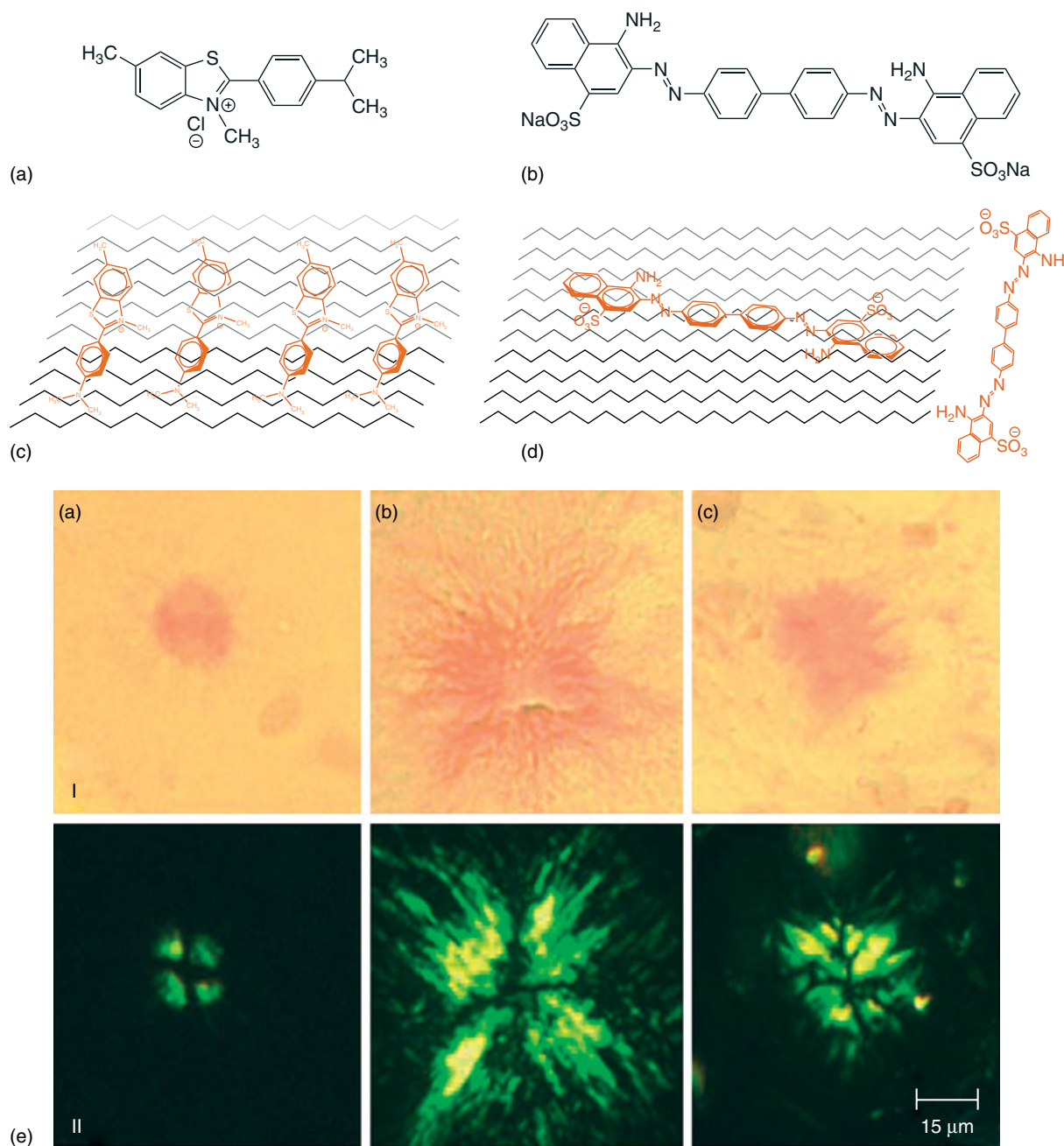
Figure 5 ThT and CR chemical structures of modes of interaction with amyloids. (a) Chemical structure of ThT. (b) Chemical structure of CR. (c) Putative mechanisms of ThT binding to amyloid fibrils. (d) Putative mechanisms of CR binding to amyloid fibrils. (e) CR-stained amyloid plaques[90]: Alzheimer's disease (A), Gerstmann–Sträussler–Scheinker disease (B), and Down's Syndrome (C). I: amyloid in linearly polarized white light; II: amyloid between crossed polarizers showing apple-green birefringence. (Panel (e) was reproduced with permission from Ref. 90. © National Academy of Sciences, U.S.A, 2003.)

for the detection of amyloids, this dye also can be used as a staining agent for fluorescence microscopy, confocal microscopy, and total-internal reflection fluorescence microscopy (TIRFM) of amyloid proteins.[102,103] The ideal concentration of the dye for spectral measurements and staining is above its critical micellar concentration, $\sim 4\,\mu M$.[98]

It has been hypothesized that ThT molecules bind to the "channels" formed in β-sheets due to the interactions between the backbone C=O from one strand and N–H from the other strand that form the fibrils.[104] The extent of ThT binding to amyloid samples depends on the accessibility of these binding grooves. There is little or no ThT binding at the initial stages of fibrillogenesis. Once

β-sheets start forming, ThT binding is initiated and it increases in proportion to the content of β-sheet in the system.

The aggregation profile monitored by ThT typically is a sigmoidal curve consisting of three different regions. The first region is called the *lag phase*, in which β-sheet structures are absent and ThT binding does not occur. This is followed by a burst phase that marks the commencement, and increase, of β-sheet formation. Eventually, a saturation phase denoting fibril maturation is observed. Typically, as the fibrils mature, lateral association of the individual filaments that compose them partially precludes ThT binding sites, resulting in lower fluorescence.[105]

ThT has been used to study fibril formation in a number of amyloidogenic proteins, including Aβ, insulin, lysozyme, α-synuclein, and β2m.[75,105–108]

Thioflavin S (ThS) is a mixture of compounds prepared by methylation of dehydrothiotoluidine with sulfonic acid and is known to stain amyloid samples.[109,110] Similar to ThT, ThS binds amyloid fibrils but not monomers, and undergoes fluorescence intensity changes and distinct spectral shift upon binding, the hyperchromic shift in the emission maxima of ThS is $\sim$45 nm.[100] Boshuizen et al. have used ThS fluorescence signal intensity change upon binding to detect fibrils formed by synthetic prion protein peptides and screen the fibril-interfering compounds. They demonstrated that the inhibitory effect of fibril formation and/or dissociation by tetracyclic compounds could be conveniently studied with this assay.[111]

ThS stained Aβ deposit in human brain tissue also could be viewed using an epifluorescence microscope.[112–114] De Felice et al. applied ThS staining to probe the volume of Aβ deposits in the hippocampi of rats and reported that nitrophenols could reduce Aβ deposition.[113]

3.3.3 *In Vivo Staining Methods*

Small molecules derived from CR and thioflavin have been developed recently for amyloid imaging, including [^{18}F] 1,1-dicyano-2-[6-(dimethylamino)-2-naphtalenyl] propene (^{18}F-FDDNP),[115] *N*-methyl [^{11}C]2-(4'-methyl-aminophenyl)-6-hydroxy-benzothiazole (^{11}C-Pittsburgh compound B (PIB)),[116] 4-*N*-methylamino-4'-hydroxys-tilbene ([^{11}C] SB13),[117] and 2-(2-[2-dimethylamino-thiazol-5-yl]ethenyl)-6-(2-[fluoro]ethoxy)-benzoxazole (^{11}C-BF-227).[118] Progress in developing amyloid imaging ligands for measuring amyloid in the brain of patients with AD is reviewed in this article.[119] Ye et al. reported that in vitro [^{3}H]-PIB, SB13, and FDDNP have high affinity binding sites on α-synuclein filament, but in vivo affinity was found to be lower. On the basis of these findings, the authors suggested that the density and/or accessibility of

α-synuclein binding sites in vivo were significantly lower than those associated with Aβ peptide lesions.[120]

4 MORPHOLOGY

Electron microscopy (EM) is a pivotal technique for studying the biological structure and function of cellular organelles and macromolecules (*see* **Electron Microscopy and Scanning Microanalysis**). High-resolution microscopic techniques, such as TEM (TEM, *see* **Scanning Electron Microscopy in Analysis of Surfaces**), STEM (STEM, *see* **Electron Microscopy and Scanning Microanalysis**), STM (STM, *see* **Scanning Tunneling Microscopy, In Situ, Electrochemical**; **Scanning Tunneling Microscopy/Spectroscopy in Analysis of Surfaces**; **Scanning Probe Microscopy, Industrial Applications of**), and AFM (AFM, *see* **Atomic Force Microscopy in Analysis of Polymers**; **Ellipsometry in Analysis of Surfaces and Thin Films**) have been useful for monitoring the morphology and structure of macromolecular assemblies involved in the pathogenesis of protein-misfolding diseases. EM allows studying morphology of noncrystalline specimens and transient intermediates. EM techniques provide nanometer to picometer resolution. General theory and EM techniques such as SEM and TEM have been reviewed by Dykstra et al.[121] Applications of TEM and STEM in the study of protein fibrillogenesis has been reviewed by Lashuel et al.[122] Gosal et al. have reviewed the application of AFM to protein and peptide self-assembly related to amyloid formation.[123]

4.1 Transmission Electron Microscopy

In TEM, a cathode ray source is used to emit and accelerate a high-voltage electron beam, which is focused by electrostatic and electromagnetic lenses. When the electrons pass through a thin and electron-transparent specimen, an image is formed from the electrons transmitted through the specimen, magnified and focused by an objective lens and appears on an imaging screen. The image carries the information about the structure of the specimen. The spatial variation in this information, which creates the image, is magnified by a series of electromagnetic lenses and detected by a fluorescent screen, photographic plate, or a charge-coupled device ((CCD) camera) (*see* **Scanning Electron Microscopy in Analysis of Surfaces**). Macromolecular specimens are typically applied onto a fine, metallic grid support coated by a thin, electron-transparent carbon film. Because
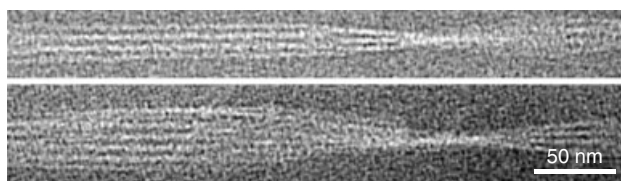
Figure 6 Two examples of cryoelectron micrographs of single $^{35Mox}A\beta(1-42)$ fibrils that were produced using recombinant $A\beta(1-42)$ peptide that contains a methionine sulfoxide at position 35. Scale bar represents 50 nm.[136] (Reproduced with permission from Ref. 136. © National Academy of Sciences, U.S.A, 2005.)

biological macromolecules have nearly identical density as that of the carbon film on the EM grids, unstained macromolecules have intrinsically low contrast when viewed by TEM. To enhance contrast and reduce image noise, several strategies, including negative staining, rotary shadowing, and cryo-EM, are used. In negative staining, the stain circumscribes the macromolecule, the shape of which is deduced from distribution of the stain, which scatters most of the electrons. In shadowing experiments, heavy metals are applied by evaporation to form a thin coating on specimens and enhance contrast. Metals may be evaporated unidirectionally either onto a static or a rotating specimen while shadowing takes place. In cryo-EM, the hydrated specimen is preserved in a thin vitreous film of ice maintained at $-180\,^\circ C$ abrogating both its sublimation and crystallization. Cryo-EM also circumvents the need for staining. These different methods have been compared by Steven and Belnap.[124] Examples for using TEM to characterize various assembly states of $A\beta$ include low molecular weight (LMW) $A\beta$,[125,126] small $A\beta$ oligomers,[127–130] paranuclei,[125,126] protofibrils,[131–134] and fibrils.[66,134,135] Cryo-EM was used to resolve the structure of $A\beta42$ fibrils, which comprised regularly spaced ($\sim$45 Å) protofilaments that twist regularly along the fibril axis (*see* Figure 6).[136] TEM was used to assess metal-induced fibril formation in α-synuclein showing that Fe and Cu ions have differential effects on α-synuclein fibrillization.[137] In another example, IAPP fibrils were shown to have a regular twist, which is found in many fibrillar preparations of amyloidogenic proteins, demonstrating the presence of more than one protofilament in fibrils.[138]

4.2 Scanning Transmission Electron Microscopy

In STEM, the illumination system includes a field emission gun, which delivers a subnanometer beam of 100-kV electrons onto a specimen. The electron beam scans the specimen and scattered electrons are collected by various types of detectors located behind the specimen. Commonly, the detectors include electron-energy-loss spectrometers (EELS), X-ray emission spectrometers,

and cathodoluminiscence spectrometers (*see* **Electron Microscopy and Scanning Microanalysis**). The image of the specimen is generated as the focused beam moves step by step over the specimen. In a thin proteinaceous specimen, the image intensity is directly proportional to the mass of the irradiated region. Therefore, following background subtraction and calibration, the protein mass and mass per length (MPL) can be determined. Of note, other biophysical techniques, including DLS (*see* Section 6.5) and AUC (*see* Section 6.4) can monitor quaternary structural alterations during formation of amyloid fibrils and enable measuring average molecular masses reflecting the distribution of an ensemble of quaternary structures in solution. However, the morphological and size heterogeneity of the intermediate structures during fibrillogenesis preclude assignment of molecular mass averages to a particular quaternary structural element. In contrast, STEM provides images of isolated and unstained specimens, allowing for accurate, quantitative mass determination of individual molecules or macromolecular assemblies.[122] A brief history STEM, description of STEM mass-mapping, and advantages and limitations of STEM have been reviewed by Wall et al.[139]

STEM is an excellent tool for characterizing the homogeneity and structural properties of transient quaternary structure intermediates in the fibril-formation pathway of amyloid proteins. The technique has been used for studies of a variety of proteins, including $A\beta$, α-synuclein, and TTR (reviewed in[122]) and to compare MPL ratio of $A\beta$ fibrils and protofibrils.[140–142]

4.3 Scanning Tunneling Microscopy

STM is a nonoptical microscopic technique that employs principles of quantum mechanics (*see* **Scanning Tunneling Microscopy, In Situ, Electrochemical**; **Scanning Tunneling Microscopy/Spectroscopy in Analysis of Surfaces**; **Scanning Probe Microscopy, Industrial Applications of**). In STM, an extremely sharp conductive tip (ideally terminating in a single atom) traces the contours of the surface of a sample with atomic resolution. An *x-y-z* piezoelectric translator controls the movement of the tip in three dimensions. When the probe is brought sufficiently close to the sample's surface and a weak voltage (a few millivolts to a few volts) is applied, a small electric current is generated by electrons tunneling across the distance between the sample and the tip. This distance is kept constant (a few nanometers) by mechanisms feeding back to the piezoelectric elements. The magnitude of the current depends exponentially on the distance between the probe and the surface. The tunneling current rapidly increases as the distance between the tip and the surface decreases. This rapid alteration in the current due to changes in

distance results in construction of an atomically resolved image when the tip scans the structure. The feedback signal applied to a piezoelectric element provides a measure of molecular surface contour. The principles and applications of STM in technology and biology have been reviewed by Hansma et al.[143]

Initial low-resolution STM studies of Aβ showed the ribbonlike filamentous nature of Aβ fibrils.[144] Later studies showed that Aβ fibrils contained laterally associated filaments that exhibited a right-handed twist.[145] In another high-resolution study, Losic et al. examined the structure of Aβ40 monomers, dimers, and oligomers on a surface of atomically flat gold.[146] Structures of $\sim$3–4 and 6–7 nm length were found, likely corresponding to monomeric and dimeric Aβ, respectively.[146] After a stock of 10-μM Aβ was incubated in phosphate-buffered saline (pH 7.4) for 24 h and diluted to 0.5 μM, larger structures, 3–4 nm wide appeared resulting from end-to-end association of monomers or dimers.[146]

4.4 Atomic Force Microscopy

AFM images high-resolution ($\leq$1 nm) topography of samples adsorbed on atomically flat smooth surfaces, typically mica. A cantilever tip scans the surface contour of the specimen and, upon contact, a repulsive force in the pN–nN range bends the cantilever upward. A laser beam focused on the end of the cantilever detects the extent of bending and the deflection of the laser is translated to force units by a photodetector. By keeping the force constant while scanning across the surface, the vertical movement of the tip generates the surface contour, which is recorded as the topography map of the sample (*see* **Atomic Force Microscopy in Analysis of Polymers**; **Ellipsometry in Analysis of Surfaces and Thin Films**).

AFM has been modified for specific applications and can be used in different modes. In contact mode, the tip is permanently in contact with the sample, whereas in "tapping mode" (also referred to as *intermittent-contact* or *dynamic-force mode*), a stiff cantilever oscillates close to the sample. Part of the oscillation extends into the repulsive regime so that the tip intermittently touches, or "taps", the surface. This mode provides good resolution on soft samples and is useful for investigation of prefibrillar species.

AFM has been used to investigate the assembly dynamics of several amyloidogenic proteins including Aβ and human IAPP.[147] IAPP fibrils comprised two protofilaments, having a 25 nm periodicity and average height of 6.8 nm.[147] An advantage of AFM over TEM is that it allows continuous monitoring of the growth of oligomers[148] and fibrils in solution.[149] Aggregation of immunoglobulin (Ig) light chains to form amyloid
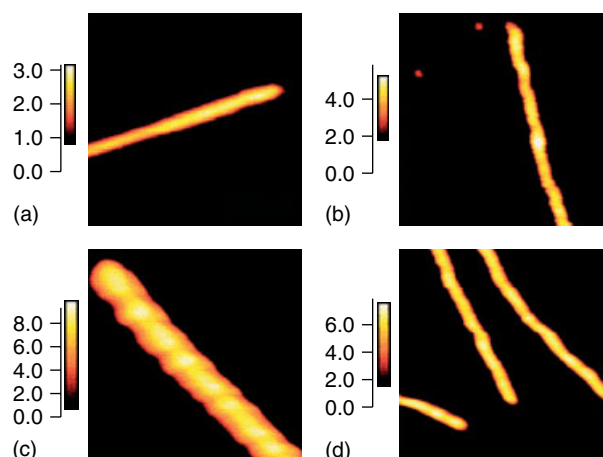

Figure 7 Typical filaments of the variable domain from amyloid fibrils of a light-chain amyloidosis protein SMA (a), protofibril (b), type-I fibril (c), and type-II fibril (d) as observed by AFM.[150] The average heights for several filaments, protofibrils, and type-I and type-II fibrils were measured to be 2.4 ± 0.3, 4.0 ± 0.4, 8.3 ± 0.9, and 5.9 ± 0.5 nm, respectively. Note that the widths depend on tip geometry and that the vertical scales are different. (Reproduced with permission from Ref. 150. © National Academy of Sciences, U.S.A, 1999.)

fibrils is a characteristic feature of light-chain amyloidosis. Time-lapsed AFM was used to monitor light-chain Ig fibril formation over time. At early times of incubation, species consistent with both monomer (2.5 ± 0.5 nm) and dimer (4.5 ± 0.5 nm) were observed. Single filaments of 2.4 nm in diameter predominated in later times for up to 12 h followed by a decrease in the next few days. The fibrils and protofibrils showed a braided structure, suggesting that their formation involves the winding of protofibrils and filaments, respectively (Figure 7).[150] Using AFM, the volume of a single PrP molecule could be determined to be 30 nm^3 corresponding well with a calculated molecular volume of 33 nm^3 by molecular dynamic simulations.[151] Recently, individual Aβ42 oligomers have been studied by AFM following dilution of the sample to concentrations that practically arrest oligomer growth. The observed high-resolution structures, corresponded to heights of $\sim$2 nm and were interpreted as folded monomers.[152]

5 TERTIARY AND QUATERNARY STRUCTURES

Because high-resolution methods, such as solution-state NMR (Section 2.1.1) or X-ray crystallography (Section 2.2) cannot be used for structural investigation of amyloidogenic protein assemblies, the tertiary and quaternary structures of these proteins often are studied using a combination of low-resolution methods,

in conjunction with methods for determination of conformation (Section 3) and morphology (Section 4). Here, we review the low-resolution study of different species along the amyloidogenic assembly pathway using ESR, H/D exchange, limited proteolysis, and several fluorescence-based methods.

5.1 Electron Spin Resonance

ESR (also called *electron paramagnetic resonance* or *EPR*, *see* **Electron Spin Resonance Spectroscopy Labeling in Peptide and Protein Analysis**; **Electron Spin Resonance Spectroscopy**) experiments were first performed by Zavoisky at the University of Kazan (Russia) in 1945.[153] ESR is an experimental technique for characterizing the energy levels of a system with unpaired electrons (such as free radicals or transition metals) in an externally applied magnetic field.[154] The basic physical concepts of ESR and NMR are similar. ESR measures the spin signals of electrons, whereas NMR measures the spin signals of atomic nuclei. More sensitive measurement in ESR, rather than NMR, can be expected because unpaired electrons do not normally exist in biological samples, making background noise very low. ESR is commonly used to investigate protein and peptide structures, particularly molecular orientation, protein dynamics, and ligand binding.

Observation of resonance requires introduction of probes containing an unpaired electron, called *spin labels*, into the molecule of interest. Spin labels used in biology are derivatives of nitroxides, small stable organic radicals, which are covalently attached to protein side chains or to metabolic substrates. Commonly used nitroxide spin labels are discussed in **Electron Spin Resonance Spectroscopy Labeling in Peptide and Protein Analysis**.

Thanks to the high sensitivity and signal-to-noise ratio in ESR spectroscopy measurement, times are substantially shorter than those required for NMR. This allows studying protein molecular dynamics in real time with millisecond resolution, which is suitable for analysis of protein folding, oligomerization, and fibril formation.

ESR has been applied by Butterfield et al. to evaluate the ability of Aβ to produce radicals, a mechanism putatively involved in Aβ-induced toxicity, using phenyl-*tert*-butylnitrone.[155] On the basis of these data, the authors suggested that radical formation by Met35 in Aβ, contributed to Aβ neurotoxicity. Additional ESR studies supported this idea and suggested that radical production by Aβ alloforms containing familial AD-related substitutions at position 22 (Dutch, Italian, Arctic) was associated with pathogenesis in these families.[156] Using similar ESR spin-trapping methods, α-synuclein has been shown to generate hydroxyl radicals in the presence of small amounts of Fe(II).[157]

Intermolecular distance analysis in Aβ fibrils,[158] and intramolecular distance measurements in Aβ monomers[159] have been reported by Török et al. and Murakami et al., respectively. Structural investigations of IAPP [160] and α-synuclein[161] fibrils using site-directed spin labeling (SDSL)-ESR study also have been reported.

5.2 Hydrogen–Deuterium Exchange

H/D exchange is a chemical reaction in which labile hydrogen atoms are substituted by deuterium atoms, typically from the solvent.[162] For protein analysis, the degree and rate of backbone amide proton exchange is useful for distinguishing regions that are exposed to the solvent, and therefore exchange more rapidly than areas that are buried in the core. The H/D exchange reaction-rate depends on the solution pH. The reaction is slow at acidic pH and can be quenched at pH $\leq$ 2.5. For studying amyloid proteins, 95% dimethyl sulfoxide (DMSO) : 5% dichloroacetate (v/v) is typically used as the quenching buffer.[163] To minimize back-exchange after quenching, the aqueous component of the quenching reagent is diluted with D_2O (typically, $D_2O : H_2O = 1 : 10$). The degree of exchange is then monitored by NMR or MS. For MS analysis, proteolysis of the sample often with pepsin is a preceding step, which is facilitated by the acidic conditions of the quenching solution.

5.2.1 Detection of Hydrogen–Deuterium Exchange by Nuclear Magnetic Resonance Spectroscopy

Commonly, heteronuclear single-quantum coherence (HSQC) spectra are used for analysis of protein H/D exchange by NMR.[164] If a hydrogen atom is replaced with deuterium, the signal in a ^{1}H NMR spectrum in the replaced region will be reduced or disappear completely, reflecting the extent of H/D exchange. Depending on the resolution of the NMR spectra, this approach may yield information on multiple specific residues simultaneously.

Wetzel and coworkers have applied H/D-NMR to studying the structure of Aβ fibrils.[165] Their study, using ^{15}N-enriched Aβ40 fibrils treated by D_2O, showed that the *N*- and *C*-termini of the peptide are accessible to the solvent in the fibril state. In contrast, the central region Lys16–Val36, except for Gly25 and Ser26, was well protected, suggesting that most of the middle domain was involved in a β-sheet structure.

Riek and coworkers proposed a 3D structure of Aβ42 fibrils based on solution NMR of dissociated Aβ42 fibrils following H/D exchange.[136] Goto's group extended the application of this method to β2m fibrils.[163]

5.2.2 Detection of Hydrogen–Deuterium Exchange by Mass Spectrometry

The protease pepsin, which specifically cleaves peptide bonds N-terminally to aromatic amino acids, is typically used prior to analysis of H/D exchange experiments by MS.[166] Pepsin is added to H/D-exchanged proteins at a ratio of 1:1 (w/w), followed by incubation for 5 min. The resultant peptide mixture is subjected either to liquid-chromatography–mass spectrometry (LC–MS), typically with electrospray ionization (ESI)[167] or to matrix-assisted laser-desorption/ionization time-of-flight (MALDI-TOF) MS. The undeuterated protein is used as a reference to clarify the mass shifts for each fragment and deuterium uptake at cleavage sites. The folding pathway and the sequences of folding or unfolding events delineated based on the detected exchange rate.

Kheterpal et al. have used H/D exchange followed by MS to study structural differences between Aβ fibrils and protofibrils stabilized by calmidazolium chloride.[167] Their study demonstrated that protofibrils undergo structural rearrangements upon maturation into fibrils and revealed structural heterogeneity in the region Aβ(20–34) of protofibrils but not fibrils.

Recently, Dobson and coworkers proposed a unique mechanism of amyloid fibril formation based on a combination of H/D exchange analyzed by both NMR and ESI–MS using fibrils formed from a Src homology 3 domain of the α-subunit of bovine phosphatidylinositol-3′-kinase. Their results have revealed that under the conditions used, exchange was dominated by a mechanism of dissociation and reassociation, which results in the recycling of molecules within the fibril population.[168] The insight obtained by the authors can be beneficial to understanding the parameters governing the behavior of proteins as they undergo denaturation and assembly into amyloid fibrils.

5.3 Limited Proteolysis

Limited proteolysis is a complimentary method to H/D exchange, aimed at mapping of protein structures by studying which regions are exposed to the surface, flexible or rigid, and estimating protein-folding dynamics. The method is based on enzymatic cleavage at sites of conformational flexibility and protection from such cleavage by stable conformations. Typically, 4–10 residues are required for a protease cleavage site. Common proteases include pepsin, which cleaves preferentially N-terminally to aromatic, but not aliphatic residues, and trypsin, which cleaves C-terminally to lysine and arginine, (except when followed by proline residues). This method is often used in combination with LC–MS under condition that limits proteolysis rate, e.g. at low enzyme–substrate ratios.

Wetzel and coworkers studied structural differences between Aβ40 monomers and fibrils by limited proteolysis using trypsin and chymotrypsin. The N-terminal proteolytic fragments, in both cases, were produced almost at the same rate for fibrillar and unaggregated Aβ40, whereas C-terminal regions of fragments in fibrils were produced more slowly than in monomers. Interestingly, the data showed that not all the N-termini were cleaved at the same rate in Aβ40 fibrils suggesting structural heterogeneity.[169]

Teplow and coworkers performed limited proteolysis of Aβ42 and Aβ40 in combination with LC–MS using an array of proteases capable of cleaving at almost every peptide bond.[170] They found a protease-resistant region (Ala21–Ala30) in both Aβ42 and Aβ40. This fragment alone, outside the full-length Aβ sequence, also was found to be resistant to proteolysis.

Myers et al. determined the conformational properties of β2m within fibrils of different morphologies by limited proteolysis of each fibril type using pepsin digestion and tandem MS.[171] The results showed that fibrils with different morphologies result in distinct digestion patterns. The long, straight fibrils formed at pH 2.5 show dramatically enhanced protection from limited proteolysis compared to shorter fibrils formed at pH 3.6.

5.4 Fluorescence Methodologies

5.4.1 Intrinsic Fluorescence

The fluorescence of the aromatic residues Trp, Tyr, and Phe is sensitive to the local environment and therefore can be used to study protein folding and assembly.[172] Most of the fluorescence emission in proteins is due to excitation of Trp residues at 280 nm. Tyr and Phe fluorescence is weaker, with intensity maxima at 274 and 257 nm, respectively.

Trp has the highest quantum yield and its emission maximum is sensitive to the polarity of its environment. Consequently, Trp is a commonly used intrinsic fluorescent probe in studying protein folding and dynamics.[172] Although Tyr is a weaker emitter than Trp, it is used often for protein analysis because of its relative abundance in nature. The Tyr emission maximum is near 305 nm and is less sensitive to the polarity of environment than Trp but more sensitive than Trp to changes in pH. Phe is the weakest fluorophore among the three and, therefore, its utility is low relative to Trp and Tyr. The fluorescence of Phe can be observed only in the absence of both Tyr and Trp.

Maji et al. have used the intrinsic fluorescence of the single Tyr residue in Aβ to probe its assembly-dependent conformational changes.[173] Tyr at position 10 in wild-type Aβ and Aβ derivatives in which Tyr10

was substituted by Phe and Tyr was introduced at position 1, 20, 30, or 40(42) were used to probe conformational dynamics during Aβ assembly. On the basis of the findings, the investigators suggested that the *C*-terminal area in Aβ42 underwent substantial conformational rearrangement during aggregation, whereas the central hydrophobic cluster (Aβ(17–21)) was essential for controlling Aβ40 aggregation. In another example, Tõugu et al. investigated the binding mode of Aβ40 to zinc or copper using a decrease in intrinsic fluorescence of Aβ40 upon binding to metals.[174]

Studies of intrinsic Tyr fluorescence in IAPP have suggested that Tyr37 and Phe23 or Phe15 form an aromatic cluster that could be important for protofilament assembly into fibrils. These results are consistent with the decreased accessibility of Tyr to quenching by iodine or acrylamide and the increased anisotropy of Tyr in fibrils.[175] Structural studies of prion, α-synuclein, Ig light-chains and apolipoproteins using intrinsic fluorescence have been reviewed by Munishkina et al.[172]

5.4.2 Fluorescence Resonance Energy Transfer

Fluorescence resonance energy transfer (FRET) is based on dipolar coupling between the emission from a fluorescence donor and the absorption of an acceptor. For FRET to occur, the emission spectrum of the donor has to overlap with the excitation spectrum of the acceptor.[176] To minimize background fluorescence from uncoupled acceptor and donor, the excitation and emission spectra of the donor and the acceptor, respectively, must have little or no overlap. Typically, FRET is manifested by a decrease in the donor emission along with an increase in acceptor emission. FRET efficiency depends on the distance between the fluorophores and, therefore, it is a useful and sensitive method for measuring intra- and intermolecular distances, monitoring protein folding, and studying protein–membrane interactions. FRET can be accomplished using the intrinsic fluorescence of aromatic residues in proteins (see Section 5.4.1) but because the fluorescence of these residues is relatively weak, high quantum yield fluorophores are typically introduced at strategic points along the sequence. Multiple parameters, including surface exposure of each fluorophore, ionic charge, solvent polarity, and overall mobility of the molecules may affect the measured fluorescence and, therefore, must be well controlled for and taken into account for distance calculations.

Glabe and coworkers reported a series of Aβ40 derivatives containing fluorophore groups, such as 5-(2-((iodoacetyl)amino)ethyl)aminonaphthylene-1-sulfonic acid or fluorescein maleimide as donors attached to Cys residues at different positions along the sequence.[177] In addition, the authors used Aβ40 derivatives containing Tyr10–Trp substitution, in order to use the Trp residue as an acceptor. The study suggested the existence of Aβ40 dimers.

Kim et al. have reported FRET experiments in which both fluorescence donor and acceptor were conjugated to Aβ(11–25) for investigation of conformational transitions during Aβ assembly.[178] Amine-reactive 5-(and-6)-carboxytetramethyl rhodamine was introduced as the donor to the *N*-terminus of Aβ(11–25) and 4-dimethylaminophenylazophenyl-4′-maleimide was attached to the *C*-terminus as the acceptor through a Cys linker. This system enabled monitoring conformational changes during the Aβ fragment assembly in real time.

FRET measurements were used to study the structure and dynamics of α-synuclein under three different conditions – at physiological pH 7.4, acidic pH 4.4, and in the presence of SDS micelles.[172,179] Trp and 3-nitro-tyrosine at six different locations in the protein were chosen as donor–acceptor pairs. The results showed that α-synuclein existed as an ensemble of compact and extended conformations under all tested conditions. In acidic solutions, the *C*-terminus of α-synuclein became more compact, whereas in the presence of SDS micelles, the *N*-terminus was more compact and the *C*-terminus was more extended.

Mukhopadhyay et al. carried out the single-molecule FRET and fluorescence correlation spectroscopy of yeast prion protein with two distinct regions, amyloidogenic *N*-terminal domain and a charged solubilizing middle region, to investigate its monomer structure and dynamics. Their results suggested that natively unfolded yeast prion consisted of an ensemble of structures having a collapsed and rapidly fluctuating *N*-terminal region juxtaposed with a more extended middle region.[180]

5.4.3 Monitoring Aggregation Using Conjugated Fluorescent Proteins

A method for monitoring protein aggregation by fusion of an amyloidogenic protein to a fluorescent protein was developed by Hecht and coworkers. The method is based on the slow folding of green fluorescent protein (GFP) and the requirement for the fully folded protein for fluorescence. When GFP is conjugated to a protein undergoing fast aggregation, e.g. Aβ42, the aggregation impedes the folding of GFP and thereby inhibits fluorescence. Hecht and coworkers used this system to screen for amino acid substitutions in Aβ that facilitate or inhibit aggregation[181] and for inhibitors of aggregation.[182] The assay is based on expression of the fusion protein in *Escherichia coli* and monitoring the green fluorescence of the colonies. A potential drawback of this approach for screening aggregation inhibitors is that successful inhibitors of Aβ42 aggregation must enter

through bacterial cell membrane in order to be recognized as a positive hit. To overcome this problem, the assay could be modified to express the fusion protein in a cell-free system.[182]

6 ASSEMBLY SIZE AND SIZE DISTRIBUTION

In this section, we discuss techniques that allow study of oligomeric distribution of proteins in equilibrating and quasi-equilibrating systems. Some of the techniques, including photo-induced cross-linking of unmodified proteins (PICUP), sodium dodecyl sulfate–polyacrylamide gel electrophoresis (SDS-PAGE), and SEC also allow preparative fractionation and purification of oligomeric assemblies, whereas others, such as DLS are used for analytical purposes only.

6.1 Sodium Dodecyl Sulfate–Polyacrylamide Gel Electrophoresis

PAGE (*see* **Gel Electrophoresis in Protein and Peptide Analysis**. In addition, for interesting historical accounts on PAGE see[183,184]) is a routine, inexpensive method enabling separation of proteins based on their electrophoretic mobility, which is governed by polypeptide charge density and/or relative molecular mass (M_r). In SDS-PAGE, protein mixtures are electrophoresed after treatment with SDS (SDS, 288.38 g mol^{-1}). SDS binds proteins via its hydrophobic dodecyl tails, leaving the sulfate groups solvent-exposed, thus creating a negatively charged "envelope" covering the protein molecules. SDS binds different polypeptides at an approximately constant mass ratio – 1.4 g SDS per gram of polypeptide. SDS binding often leads to denaturing secondary and nondisulfide-linked tertiary structures, resulting in electrophoretic migration rates governed largely by the polypeptide chain length (i.e. M_r). In the absence of SDS, proteins of different mass-to-charge ratio electrophorese distinctly and protein conformation and folding also affect electrophoretic mobility.

Although SDS-PAGE is generally an excellent analytical and preparative method in protein analysis (*see* **Gel Electrophoresis in Protein and Peptide Analysis**), importantly, the effect of SDS on all proteins is not equivalent.[185] Different proteins, different conformations of the same protein,[186] or truncated versions of certain proteins[187] may not bind stoichiometric amounts of SDS. In addition, in certain cases, SDS can induce or stabilize secondary and quaternary structures rather than denaturing them.[186,188,189] Also, SDS may cause dissociation of protein assemblies or conversely, induce protein self-association, depending on

the specific protein studied.[189–192] For example, Aβ42-derived "globulomers" are oligomeric species produced by incubating Aβ42 in the presence of 0.2% SDS.[193] Apparent electrophoretic fractionation of monomeric or oligomeric components in a protein mixture does not necessarily indicate existence of such components prior to SDS treatment. Examples of this shortcoming of SDS-PAGE have been reported in its applications to studies of Aβ[194] and α-synuclein.[195]

Aβ is an amphipathic protein known to form SDS-stable oligomers. In fact, SDS-induced assembly of Aβ into insoluble aggregates has been capitalized on to purify Aβ from brain homogenates.[196] When treated with SDS, Aβ assembles rapidly into high-molecular-mass aggregates.[194] During electrophoresis of Aβ40, these aggregates dissociate completely and only a monomer is observed following staining, whereas electrophoresis of Aβ42 yields apparent trimeric and tetrameric components (Figure 8[125]).[126] In addition, essentially identical monomer–trimer–tetramer distributions are observed when different preparations of Aβ42, including monomeric, oligomeric, and fibrillar Aβ42, are analyzed by SDS-PAGE,[197] demonstrating that the treatment with SDS, rather than the initial assembly state, determines the electrophoretic mobility of Aβ42. In a urea-containing SDS-PAGE system, Aβ and truncated versions thereof do not obey the law of mass–mobility relationship, likely because Aβ–SDS binding is proportional to the sum of the hydrophobicity indices, rather than the number, of constituent amino acids.[187]
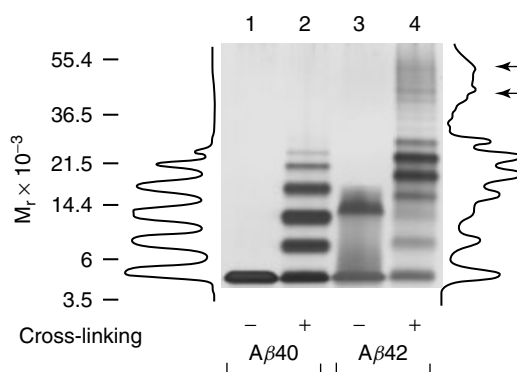

Figure 8 SDS-PAGE with or without PICUP analysis of Aβ40 and Aβ42. Aggregate-free Aβ40 and Aβ42 were prepared by SEC [125] and either mixed with Tricine sample buffer or cross-linked immediately following their isolation. SDS-PAGE analysis was followed by silver staining. Noncross-linked (lanes 1 and 3) or cross-linked (lanes 2 and 4) Aβ40 and Aβ42 are shown. Densitometric intensity profiles of lanes 2 (cross-linked Aβ40) and 4 (cross-linked Aβ42) are shown on the left and right, respectively. Arrows next to lane 4 indicate intensity maxima corresponding to presumptive dodecamer and octadecamer species. (Reproduced with permission from Ref. 125. © National Academy of Sciences, U.S.A, 2003.)

Both human and rat α-synuclein have shown aberrant electrophoretic mobility upon SDS-PAGE, whereas artifactual SDS-PAGE-induced high-molecular-mass components were not observed when the samples were analyzed by SEC.[195] Thus, despite its wide use and high resolution, SDS-PAGE is not a reliable method for size determination of certain proteins (e.g. α-synuclein) or noncovalently stabilized protein assemblies (e.g. Aβ oligomers).

6.2 Photo-Induced Cross-Linking of Unmodified Proteins

PICUP stabilizes oligomer populations by covalent cross-linking and provides snapshots of homo- or hetero-molecular interactions that exist before cross-linking. In a metastable protein mixture, oligomers dissociate into monomers and associate into larger assemblies continuously in quasi-equilibrium. PICUP, when combined with SDS-PAGE or SEC, enables visualization and analysis of the size distribution of metastable protein assemblies.[198] PICUP involves photo-oxidation of Ru^{2+} in a tris(bipyridyl)Ru(II) complex (Ru(Bpy)) to Ru^{3+} by irradiation with visible light in the presence of an electron acceptor. Ru^{3+} is a strong one-electron oxidizer capable of abstracting an electron from a neighboring protein molecule, generating a protein radical.[198,199] Radicals are unstable, highly reactive species and, therefore, disappear rapidly through a variety of intra- and intermolecular reactions. A radical may utilize the high energy of an unpaired electron to react with another protein monomer forming a dimeric radical, which may subsequently lose a hydrogen atom and form a stable, covalently linked dimer. The dimer may then react further through a similar mechanism with monomers or other dimers to form higher order oligomers. Some of the advantages of this method, as opposed to other chemical cross-linking methods,[200] are that PICUP-generated covalent bonds between closely interacting polypeptide chains occur within $\leq 1\,s$ exposure to nondestructive visible light, without pre facto chemical modifications of the native sequence, and without using spacers. Furthermore, PICUP enables cross-linking of proteins within wide pH and temperature ranges, including physiological parameters.

PICUP was originally developed to study stable protein complexes.[199] The method was applied later to quantitative study of metastable amyloid protein assemblies, including Aβ,[201] calcitonin,[198] prion, and disease-associated PrP^{Sc},[192] and α-synuclein.[202] Using PICUP, the effect of amino acid sequence modifications on the quaternary structure and the relationship between primary and quaternary structures of metastable protein oligomers can be investigated.[198] For example, Aβ40

and Aβ42 were found to form distinct oligomer size distributions, each of which was affected distinctly by a subset of structural modifications in the Aβ sequence.[201] Furthermore, PICUP was used to show that aggregates of rPrP and PrP^{Sc} were linked at interacting surfaces via amino acid side chains. Specific intermolecular cross-linking of PrP^{Sc} was achieved even in crude brain homogenates, and cross-linking did not alter the level of infectivity of PrP^{Sc}, indicating that PICUP-induced covalent linkage of PrP^{Sc} did not abolish surface interactions important for prion propagation.[192] When PICUP was applied to studying early events of α-synuclein oligomerization, it was found that soluble α-synuclein existed as an equilibrium comprising monomers, dimers, and trimers, and the N-terminal amphipathic region was proposed to be required for oligomerization.[202]

The mechanism, instrumentation, protocol, and limitations of PICUP were discussed in detail elsewhere.[198,199]

6.3 Size-Exclusion Chromatography

SEC (also called *gel permeation chromatography* and *gel filtration chromatography*) (*see* **Size-exclusion Chromatography of Polymers**; **Biopolymer Chromatography**) fractionates solutes based on their Stokes radii, i.e. hydrodynamic volumes (which can be correlated with molar mass).[203] SEC is used to determine molar mass averages and molar mass distributions of solutes. SEC separation is achieved using a stationary phase comprising a porous matrix. In principle, limited accessibility of the pores within the particles of the stationary phase causes larger molecules to interact less with the solid phase and elute faster than smaller molecules. SEC affords an SDS-independent separation mechanism and covers a molecular mass range of $\sim 10^3 - 10^6$ Da. However, SEC provides lower resolution than SDS-PAGE or mass spectrometric techniques, and molecular-mass estimations of polypeptides can be inaccurate if the elution profiles are sensitive to protein conformation.

Analytical and preparative SEC are used extensively in the study of amyloid proteins. SEC can distinguish between protofibrils (PF) and small oligomers of Aβ[66] and other aggregation-prone proteins, making it a useful technique for studying the kinetics involved in conversion of LMW oligomers to PF (or dissociation of PF into LMW oligomers). In addition to its use as an analytical method,[204] SEC has been used extensively to purify fractions of particular assemblies.[125,131–133,205,206] SEC along with other complementary techniques, including CD, ThT-binding fluorescence, and DLS were used to investigate the propensity of the various mutants of Cu/Zn superoxide dismutase 1 (SOD1) in the apo- and Zn-bound protein in comparison to the wild-type SOD1.[207] There are about 100 single-point mutations of SOD1

reportedly related to the familial form of amyotrophic lateral sclerosis. Description of the basic instrumentation and utilization of SEC for preparation of aggregate-free Aβ was published previously.[208]

6.4 Analytical Ultracentrifugation

AUC is a versatile technique used extensively to characterize hydrodynamic and thermodynamic properties of proteins and other macromolecules (*see* **Centrifugation in Particle Size Analysis**; **Sedimentation in Particle Size Analysis**). Conceptually, AUC allows real-time quantitative analysis of spatial redistribution of analytes in solution under an ultracentifugal force field. Unlabeled and unmodified proteins can be analyzed by AUC in a wide range of excipient conditions, obviating analyte–matrix interactions such as those occurring during SEC. Because molecular frictional forces oppose the centrifugal force, sedimentation depends, in addition to other parameters, on the hydrodynamic properties of the molecules, providing low-resolution information on the structure of protein complexes, and enabling detection of conformational alterations.

Coupled with data-analysis software, AUC can determine sample purity and molecular mass in solution, measure sedimentation and diffusion coefficients, characterize assembly–disassembly mechanisms of complex analytes, determine subunit stoichiometry, detect and characterize macromolecular conformational changes, and measure equilibrium constants and thermodynamic parameters for self- and hetero-associating assemblies.

Often, two types of AUC experiments are performed – sedimentation velocity (SV) and sedimentation equilibrium (SE). Typically, SV is conducted at relatively high rotor speeds. In SV experiments, each protein species in a mixture forms a unique boundary and sediments at a characteristic speed governed by its molecule mass, size, and shape. The velocity and shape of the moving concentration boundary is used to estimate the sedimentation coefficient, diffusion coefficient, molecular mass, and equilibrium constants of interacting species. SE experiments are operated at relatively low rotor speeds. The sedimentation of proteins under lower centrifugal forces than SV experiments is opposed by the diffusion, and eventually when equilibrium is reached, a time-invariant exponential concentration gradient is established throughout the centrifuge cell. The concentration gradient of proteins at equilibrium has been used widely to determine the molecular weight, stoichiometry, binding affinity, and virial coefficient of hetero-interacting or self-associating systems.

AUC combines an ultracentrifuge, a multicompartmental rotor, and an optical system for detection of analyte concentration. The optical detection system is triggered by the revolution of the rotor, allowing acquisition of data only during the extremely short intervals when a particular sample assembly aligns within the optical path. Two commercially available optical detection systems, dual-beam ultraviolet/visible spectrophotometers and highly sensitive laser interferometers capable of recording the refractive index, are used widely.

SV and SE AUC have been used to analyze size distribution of various components of amyloidogenic assemblies.[209–211] Aβ-derived diffusible ligands (ADDLs), which are soluble Aβ42-derived prefibrillar neurotoxic assemblies, have been shown to contain a high-molecular-mass component with estimated mass of 175 kDa by SV and 120–540 kDa by SE experiments.[197] Using SE, Huang et al. have reported that Aβ40 existed as an equilibrium mixture of monomers, dimers, and tetramers at neutral pH. However, other equilibria, including monomer–dimer, monomer–trimer, or monomer–tetramer, could not be ruled out hindering precise determination of the oligomerization state of the peptide by this method.[212] AUC along with CD spectroscopy and chemical cross-linking were used to characterize the preamyloid state of recombinant PrP$_{89-230}$. SE experiments showed that the preamyloid form of recombinant PrP existed in a monomer–dimer equilibrium.[68] SE and SV AUC were used to characterize the quaternary structural requirements for TTR amyloidogenic intermediates, which lead to fibril formation and cause senile systemic amyloidosis and familial amyloid polyneuropathy.[210]

6.5 Dynamic Light-Scattering Spectroscopy

DLS, also known as *quasielastic light-scattering, photon-correlation spectroscopy*, or *intensity fluctuation spectroscopy* (*see* **Photon Correlation Spectroscopy in Particle Sizing**; **Light Scattering, Classical: Size and Size Distribution Characterization**; **Turbidimetry in Particle Size Analysis**; **Diffraction in Particle Size Analysis**), is a noninvasive, nondestructive, quantitative, optical method for determining diffusion coefficients of particles (0.1–3000-nm size range[213]) undergoing Brownian motion in solution or suspension. DLS measures the temporal fluctuations of light scattering by solute particles as a function of time (over $10^{-7}–1$ s). Temporal fluctuations in the intensity of the scattered light relate to the rate of Brownian motion, which is correlated to the diffusion coefficient, D, and the radii of the particles according to the Stokes–Einstein equation:[214,215]

$$D = \frac{k_B T}{6\pi \eta R_h} = \frac{k_B T}{3\pi \eta D_h} \qquad (1)$$

where k_B is Boltzmann's constant, T is the absolute temperature, η is the viscosity of the suspending liquid, and R_h and D_h are the hydrodynamic radius and diameter, respectively. Knowledge of diffusion coefficient of molecules allows determination of molecular features, including size and flexibility. Temporal changes in these parameters provide information about the kinetics and structural transitions occurring, e.g. during protein assembly–disassembly processes. In a polydisperse mixture, a distribution of diffusion coefficients is obtained.

DLS has an intrinsic bias for large aggregates because the intensity of the scattered light is proportional to the square of the particle mass.[216] Therefore, DLS is well suited to measure minute amounts of aggregated proteins (<0.01% by weight) on the background of monomers and small oligomers. For large or extended proteins (rodlike/unfolded), scattering varies significantly with angle.[217] Determining scattering at additional angles by multiangle laser light scattering (MALLS) allows direct measurements of masses up to the MDa range. Because the light-scattering signal is directly proportional to protein concentration and molecular mass, a combination of DLS signal and concentration measurements using refractive index or absorbance, allows calculation of the molecular mass of each component when proteins are fractionated chromatographically. DLS can resolve the monomeric and dimeric state of a protein if the shape of the protein is known, but it cannot distinguish among small oligomers when their hydrodynamic radii differ by less than a factor of 2[218] or between, for example, a compact dimer and an extended monomer. Consequently, DLS is less useful for analyzing individual small oligomers than SEC-MALLS, PICUP coupled with SDS-PAGE, or SV AUC.

DLS has been applied to structural studies of multiple amyloidogenic proteins, including insulin,[219] calcitonin,[220] and the model protein barstar.[70] Detailed accounts of the theory, instrumentation, practice, and data analysis of DLS applied to the study of Aβ have been reviewed by Lomakin et al.[216,221,222]

Because DLS allows monitoring protein assembly noninvasively, it has been used widely to study Aβ aggregation and assembly processes.[125,132,134,223–226] Solution state and size distribution of ADDLs has been assessed recently by Hepler et al. using SEC coupled with MALLS.[197] Walsh et al. reported studies using DLS and other techniques examining early stages of Aβ oligomerization and characterization of Aβ intermediates during fibrillogenesis.[131] Shape and size of discrete oligomeric species, which are formed on the pathway of oxidative prion aggregation in vitro, also were characterized using DLS along with other complementary methods.[227]

6.6 Ion-Mobility Spectrometry–Mass Spectrometry

When coupled with MS (*see* **Mass Spectrometry: Overview and History**), IMS (*see* **Ion Mobility Spectrometry in Forensic Science**), which separates ions based on both their mass-to-charge ratio and their 3D structure, is a powerful analytical method for investigating molecular structures in complex samples.[228] IMS–MS can resolve molecules of identical mass-to-charge (m/z) ratios that have different collision cross-sections (e.g. different assembly states or conformations) and/or charge states. An IMS–MS instrument performs five basic processes: sample introduction, compound ionization, ion-mobility separation, mass separation, and ion detection (*see* Figure 9).[229] Four types of IMS are used: drift-time, aspiration, differential, and traveling-wave. Drift-time IMS is operated under either ambient pressure or reduced-pressure conditions. Aspiration and differential IMS are operated under ambient pressure, whereas the traveling-wave IMS is performed under reduced-pressure conditions. Each of these IMS setups can be interfaced to a variety of mass spectrometers, including time-of-flight (*see* **Time-of-flight Mass Spectrometry**; **Mass Spectrometry: Overview and History**), quadrupole (*see* **Quadrupole Ion Trap Mass Spectrometer**; **Mass Spectrometry: Overview and History**), ion-trap (*see* **Quadrupole Ion Trap Mass Spectrometer**; **Mass Spectrometry: Overview and History**), ion-cyclotron (*see* **Electron Ionization Mass Spectrometry**; **Mass Spectrometry: Overview and History**), or magnetic-sector mass spectrometers (*see* **Mass Spectrometry: Overview and History**). In traditional drift-time IMS, ions are carried by a weak, uniform electric field through a drift cell in which they collide at low velocity with a low-pressure inert gas such that the collision thermal energy due to the buffer gas is greater than the energy the ions obtain from the electric field. Under this principal condition, ions have energies similar to that of the buffer gas so that they undergo a directional diffusion process. Under these low-field conditions, the drift velocity of ions is directly proportional to the electric field but inversely proportional to their collision cross-section. This proportionality is defined by ion-mobility constant (K), which is related to ionic cross-section by

$$K = \left(\frac{3q}{16N}\right)\sqrt{\left(\frac{2\pi}{kT}\right)}\sqrt{\left(\frac{m+M}{mM}\right)}\left(\frac{1}{\Omega}\right) \qquad (2)$$

where q is the ion charge, N is the number density of the buffer gas, k is Boltzmann's constant, T is the absolute temperature, m is the mass of the buffer gas, M is the mass of the ion, and Ω is the collision cross-section of the ion.[228] Thus, in the case of a mixture of protein assemblies, conformers/ions with compact structures and
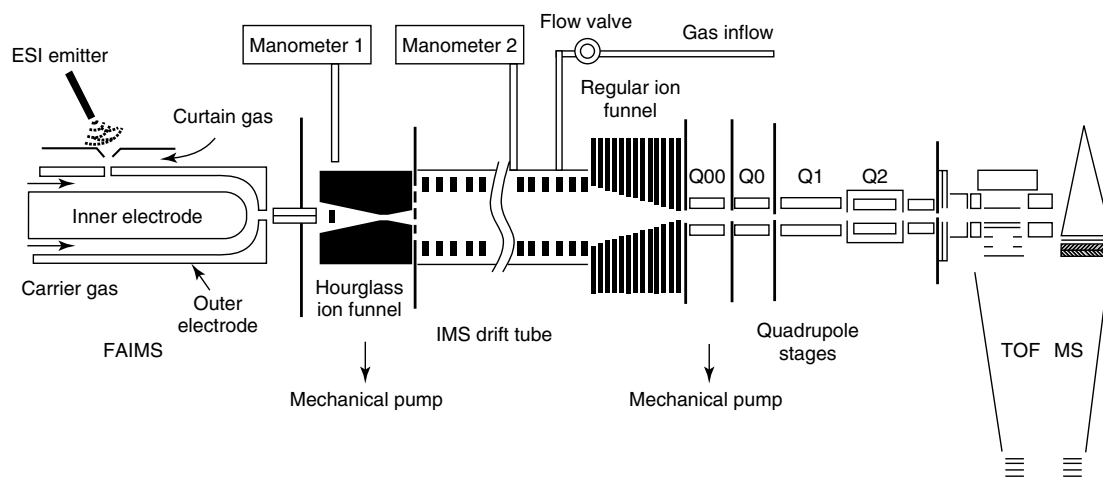
Figure 9 A scheme of an ESI-FAIMS/IMS/Q-TOF MS instrument.[229] ESI, FAIMS, Q00–Q2, and TOF MS denote electrospray ionization, field-asymmetric waveform ion-mobility spectrometer, quadrupole stages 00–2, and time-of-flight mass spectrometer, respectively. (Reproduced from Ref. 229. © American Chemical Society, 2005.)

smaller cross-section have higher mobility and drift faster through the cell than ions with larger cross-sections. The ions exit the drift cell, pass through a mass filter, and are detected as a function of time, producing a temporal arrival distribution. The traditional drift-time IMS is the only type allowing measurement of collision cross-section of ions.

Detailed discussion of the instrumentation and theory of IMS–MS, various types of IMS–MS interfaced to different types of mass spectrometers, and selected IMS–MS applications have been reviewed elsewhere.[228,230]

Protein oligomers often have identical m/z ratio (i.e. a singly charged monomer has the same m/z as a doubly charged dimer, triply charged trimer, etc.). IMS–MS analysis can resolve these species yielding an oligomer size distribution. IMS–MS studies of $A\beta$ have shown that freshly prepared LMW $A\beta40$ contained monomers, dimers, trimers, and tetramers, whereas similarly prepared solutions of $A\beta42$ comprised oligomers up to a dodecamer.[231] These results accord with earlier observations of distinct oligomer size distributions of $A\beta40$ and $A\beta42$ by PICUP[125] and may explain differences in neurotoxic effects of the two $A\beta$ alloforms. IMS interfaced with ESI-MS was used to analyze α-synuclein[232] and β_2m[233] under different pH conditions and study various protein conformers. Different β_2m conformers were found to co-exist in the solution and could be detected and analyzed by ESI field-asymmetric ion-mobility spectrometry (ESI-FAIMS), consistent with observations of their folding behavior described by complimentary biophysical techniques, including CD and NMR.[233] Utilization of gas-phase approaches such as IMS has led to accumulation of

extensive evidence that ESI (and to some extent MALDI) can produce ions that retain key structural aspects of proteins in solution.[234] In particular, the dependence of protein conformation on solution conditions (e.g. pH and excipient composition) in IMS and FAIMS shows that gas-phase measurements can concord with protein conformations in solution.[234] Furthermore, 2D FAIMS–IMS separations coupled with MS revealed many more protein conformations (including some lowly abundant conformations) than either FAIMS or IMS alone used in the study of cytocrome c and ubiquitin,[234] suggesting that IMS–MS and IMS–IMS–MS offer great potential in the dissection of protein conformational dynamics, a feat currently unachievable by other biophysical techniques.

ACKNOWLEDGMENTS

ABBREVIATIONS AND ACRONYMS

2DIR	Two-dimensional infrared
3D	Three-dimensional
β2m	β_2-microglobulin
Aβ	Amyloid β-protein
AD	Alzheimer's disease
ADDLs	Aβ-derived diffusible ligands
AFM	Atomic force microscopy
ATR-FTIR	Attenuated total-internal reflection Fourier transform infrared
AUC	Analytical ultracentrifugation
CCD	Charge-coupled device
CD	Circular dichroism
CP	Cross polarization
CR	Congo red
DLS	Dynamic light scattering
DMSO	Dimethyl sulfoxide
EELS	Electron-energy-loss spectrometers
EM	Electron microscopy
EPR	Electron paramagnetic resonance
ESI	Electrospray ionization
ESR	Electron spin resonance
EXAFS	Extended X-ray absorption fine structure
FAIMS	Field-asymmetric ion-mobility spectrometry
FRET	Fluorescence resonance energy transfer
FTIR	Fourier transform infrared spectroscopy
GFP	Green fluorescent protein
HCC	Human cystatin C
H/D	Hydrogen–deuterium
HSQC	Heteronuclear single-quantum coherence
IAPP	Islet amyloid polypeptide
LC–MS	Liquid-chromatography–mass spectrometry
Ig	Immunoglobulin
IMS	Ion-mobility spectrometry
LMW	Low molecular weight
MALDI-TOF	Matrix-assisted laser-desorption ionization/time of flight
MALLS	Multiangle laser light scattering
MAS	Magic-angle spinning
NMR	Nuclear magnetic resonance
MPL	Mass per length
NOE	Nuclear Overhauser effect
PD	Parkinson's disease
PICUP	Photo-induced cross-linking of unmodified proteins
PF	Protofibrils
SANS	Small-angle neutron scattering
SDS-PAGE	Sodium dodecyl sulfate–polyacrylamide gel electrophoresis
SDSL	Site-directed spin labeling
SE	Sedimentation equilibrium
SEC	Size-exclusion chromatography
SOD1	Superoxide dismutase 1
ssNMR	Solid-state NMR
SMA	Immunoglobulin light chain variable domains from patients with these initials
STEM	Scanning transmission electron microscopy
STM	Scanning tunneling microscopy
SV	Sedimentation velocity
TEM	Transmission electron microscopy
ThT	Thioflavin T
ThS	Thioflavin S
TIRFM	Total-internal reflection fluorescence microscopy
TTR	Transthyretin
UV	Ultraviolet
XANES	X-ray absorption near-edge structure
XAS	X-ray absorption spectroscopy

RELATED ARTICLES

Absorption Techniques in X-ray Spectrometry
Atomic Force Microscopy in Analysis of Polymers
Biopolymer Chromatography
Centrifugation in Particle Size Analysis
Circular Dichroism and Linear Dichroism
Circular Dichroism in Analysis of Biomolecules
Diffraction in Particle Size Analysis
Electron Ionization Mass Spectrometry
Electron Microscopy and Scanning Microanalysis
Electron Spin Resonance Spectroscopy
Electron Spin Resonance Spectroscopy Labeling in Peptide and Protein Analysis
Ellipsometry in Analysis of Surfaces and Thin Films
Fourier Transform Infrared Spectroscopy in Peptide and Protein Analysis
Gel Electrophoresis in Protein and Peptide Analysis
Infrared Spectroscopy in Clinical Chemistry
Infrared Spectroscopy: Introduction
Infrared Spectroscopy of Biological Applications
Ion Mobility Spectrometry in Forensic Science
Light Scattering, Classical: Size and Size Distribution Characterization
Mass Spectrometry: Overview and History
Neutron Scattering in Analysis of Polymers and Rubbers
Nuclear Magnetic Resonance Instrumentation

REFERENCES

1. R.S. Harrison, P.C. Sharpe, Y. Singh, D.P. Fairlie, 'Amyloid Peptides and Proteins in Review', *Rev. Physiol. Biochem. Pharmacol.*, **159**, 1–77 (2007).

2. G. Merlini, P. Westermark, 'The Systemic Amyloidoses: Clearer Understanding of the Molecular Mechanisms Offers Hope for More Effective Therapies', *J. Intern. Med.*, **255**, 159–178 (2004).

3. O.S. Makin, L.C. Serpell, 'Examining the Structure of the Mature Amyloid Fibril', *Biochem. Soc. Trans.*, **30**, 521–525 (2002).

4. O.S. Makin, L.C. Serpell, 'Structures for Amyloid Fibrils', *FEBS J.*, **272**, 5950–5961 (2005).

5. C.M. Dobson, 'Principles of Protein Folding, Misfolding and Aggregation', *Semin. Cell Dev. Biol.*, **15**, 3–16 (2004).

6. M.T. Pastor, N. Kummerer, V. Schubert, A. Esteras-Chopo, C.G. Dotti, M. Lopez de la Paz, L. Serrano, 'Amyloid Toxicity is Independent of Polypeptide Sequence, Length and Chirality', *J. Mol. Biol.*, **375**, 695–707 (2008).

7. S.T. Ferreira, F.G. De Felice, A. Chapeaurouge, 'Metastable, Partially Folded States in the Productive Folding and in the Misfolding and Amyloid Aggregation of Proteins', *Cell Biochem. Biophys.*, **44**, 539–548 (2006).

8. M. Stefani, C.M. Dobson, 'Protein Aggregation and Aggregate Toxicity: New Insights into Protein Folding, Misfolding Diseases and Biological Evolution', *J. Mol. Med.*, **81**, 678–699 (2003).

9. C.M. Dobson, 'Protein Folding and Misfolding', *Nature*, **426**, 884–890 (2003).

10. M. Bucciantini, E. Giannoni, F. Chiti, F. Baroni, L. Formigli, J. Zurdo, N. Taddei, G. Ramponi, C.M. Dobson, M. Stefani, 'Inherent Toxicity of Aggregates Implies a Common Mechanism for Protein Misfolding Diseases', *Nature*, **416**, 507–511 (2002).

11. Y. Fezoui, D.B. Teplow, 'Kinetic Studies of Amyloid β-Protein Fibril Assembly. Differential Effects of α-Helix Stabilization', *J. Biol. Chem.*, **277**, 36948–36954 (2002).

12. S. Pasternak, B.A. Wright, N. Walsh, 'Soft Tissue Amyloidoma of the Extremities: Report of a Case and Review of the Literature', *Am. J. Dermatopathol.*, **29**, 152–155 (2007).

13. A.T. Brünger, 'X-ray Crystallography and NMR Reveal Complementary Views of Structure and Dynamics', *Nat. Struct. Biol.*, **4**(Suppl), 862–865 (1997).

14. M. Zeeb, J. Balbach, 'Protein Folding Studied by Real-Time NMR Spectroscopy', *Methods*, **34**, 65–74 (2004).

15. H.J. Dyson, P.E. Wright, 'Unfolded Proteins and Protein Folding Studied by NMR', *Chem. Rev.*, **104**, 3607–3622 (2004).

16. R. Riek, P. Güntert, H. Döbeli, B. Wipf, K. Wüthrich, 'NMR Studies in Aqueous Solution Fail to Identify Significant Conformational Differences between the Monomeric Forms of two Alzheimer Peptides with Widely Different Plaque-Competence, $A\beta(1–40)^{ox}$ and $A\beta(1–42)^{ox}$', *Eur. J. Biochem.*, **268**, 5930–5936 (2001).

17. G. Esposito, A. Corazza, P. Viglino, G. Verdone, F. Pettirossi, F. Fogolari, A. Makek, S. Giorgetti, P. Mangione, M. Stoppini, V. Bellotti, 'Solution Structure of β_2-Microglobulin and Insights into Fibrillogenesis', *Biochim. Biophys. Acta*, **1753**, 76–84 (2005).

18. Y.H. Sung, D. Eliezer, 'Secondary Structure and Dynamics of Micelle Bound β- and γ-Synuclein', *Protein Sci.*, **15**, 1162–1174 (2006).

19. S. Tomaselli, V. Esposito, P. Vangone, N.A. van Nuland, A.M. Bonvin, R. Guerrini, T. Tancredi, P.A. Temussi, D. Picone, 'The α-to-β Conformational Transition of Alzheimer's Aβ-(1–42) Peptide in Aqueous Media is Reversible: A Step by Step Conformational Analysis Suggests the Location of β Conformation Seeding', *ChemBioChem*, **7**, 257–267 (2006).

20. H. Shao, S. Jao, K. Ma, M.G. Zagorski, 'Solution Structures of Micelle-Bound Amyloid β-(1–40) and β-(1–42) Peptides of Alzheimer's Disease', *J. Mol. Biol.*, **285**, 755–773 (1999).

21. P.K. Mandal, J.W. Pettegrew, D.W. McKeag, R. Mandal, 'Alzheimer's Disease: Halothane Induces Aβ Peptide to Oligomeric Form – Solution NMR Studies', *Neurochem. Res.*, **31**, 883–890 (2006).

22. M. Coles, W. Bicknell, A.A. Watson, D.P. Fairlie, D.J. Craik, 'Solution Structure of Amyloid β-Peptide(1–40) in a Water-Micelle Environment. Is the Membrane-Spanning Domain where we think it is?' *Biochemistry*, **37**, 11064–11077 (1998).

23. J. Talafous, K.J. Marcinowski, G. Klopman, M.G. Zagorski, 'Solution Structure of Residues 1–28 of the Amyloid β-Peptide', *Biochemistry*, **33**, 7788–7796 (1994).

24. K. Kirshenbaum, V. Daggett, 'Sequence Effects on the Conformational Properties of the Amyloid β-(1–28) Peptide: Testing a Proposed Mechanism for the α–β Transition', *Biochemistry*, **34**, 7640–7647 (1995).

25. K. Kirshenbaum, V. Daggett, 'pH-Dependent Conformations of the Amyloid β-(1–28) Peptide Fragment Explored using Molecular Dynamics', *Biochemistry*, **34**, 7629–7639 (1995).

26. L. Hou, H. Shao, Y. Zhang, H. Li, N.K. Menon, E.B. Neuhaus, J.M. Brewer, I.J. Byeon, D.G. Ray, M.P. Vitek, T. Iwashita, R.A. Makula, A.B. Przybyla, M.G. Zagorski, 'Solution NMR Studies of the Aβ (1–40) and Aβ (1–42) Peptides Establish that the Met35 Oxidation State Affects the Mechanism of Amyloid Formation', *J. Am. Chem. Soc.*, **126**, 1992–2005 (2004).

27. Y. Yan, C. Wang, 'Aβ42 is More Rigid than Aβ40 at the C Terminus: Implications for Aβ Aggregation and Toxicity', *J. Mol. Biol.*, **364**, 853–862 (2006).

28. A. Naito, M. Kamihira, R. Inoue, H. Saito, 'Structural Diversity of Amyloid Fibril Formed in Human Calcitonin as Revealed by Site-Directed 13C Solid-State NMR Spectroscopy', *Magn. Reson. Chem.*, **42**, 247–257 (2004).

29. M. Kamihira, A. Naito, S. Tuzi, A.Y. Nosaka, H. Saito, 'Conformational Transitions and Fibrillation Mechanism of Human Calcitonin as Studied by High-Resolution Solid-State ^{13}C NMR', *Protein Sci.*, **9**, 867–877 (2000).

30. R. Tycko, Y. Ishii, 'Constraints on Supramolecular Structure in Amyloid Fibrils from Two-Dimensional Solid-State NMR Spectroscopy with Uniform Isotopic Labeling', *J. Am. Chem. Soc.*, **125**, 6606–6607 (2003).

31. P.T. Lansbury, Jr, P.R. Costa, J.M. Griffiths, E.J. Simon, M. Auger, K.J. Halverson, D.A. Kocisko, Z.S. Hendsch, T.T. Ashburn, R.G. Spencer, B. Tidor, R.G. Griffin, 'Structural Model for the β-Amyloid Fibril Based on Interstrand Alignment of an Antiparallel-Sheet Comprising a C-Terminal Peptide', *Nat. Struct. Biol.*, **2**, 990–998 (1995).

32. J.J. Balbach, A.T. Petkova, N.A. Oyler, O.N. Antzutkin, D.J. Gordon, S.C. Meredith, R. Tycko, 'Supramolecular Structure in Full-Length Alzheimer's β-Amyloid Fibrils: Evidence for a Parallel β-Sheet Organization from Solid-State Nuclear Magnetic Resonance', *Biophys. J.*, **83**, 1205–1216 (2002).

33. A. Naito, I. Kawamura, 'Solid-State NMR as a Method to Reveal Structure and Membrane-Interaction of Amyloidogenic Proteins and Peptides', *Biochim. Biophys. Acta*, **1768**, 1900–1912 (2007).

34. H. Heise, 'Solid-State NMR Spectroscopy of Amyloid Proteins', *ChemBioChem*, **9**, 179–189 (2008).

35. R. Tycko, 'Characterization of Amyloid Structures at the Molecular Level by Solid State Nuclear Magnetic Resonance Spectroscopy', *Methods Enzymol.*, **413**, 103–122 (2006).

36. R. Tycko, 'Molecular Structure of Amyloid Fibrils: Insights from Solid-State NMR', *Q. Rev. Biophys.*, **39**, 1–55 (2006).

37. R. Tycko, 'Solid-State NMR as a Probe of Amyloid Structure', *Protein Pept. Lett.*, **13**, 229–234 (2006).

38. R. Tycko, 'Progress Towards a Molecular-Level Structural Understanding of Amyloid Fibrils', *Curr. Opin. Struct. Biol.*, **14**, 96–103 (2004).

39. A.T. Petkova, W.M. Yau, R. Tycko, 'Experimental Constraints on Quaternary Structure in Alzheimer's β-Amyloid Fibrils', *Biochemistry*, **45**, 498–512 (2006).

40. A.A. Chernov, 'Protein Crystals and their Growth', *J. Struct. Biol.*, **142**, 3–21 (2003).

41. C. Rosano, S. Zuccotti, M. Bolognesi, 'The Three-Dimensional Structure of β2 Microglobulin: Results from X-ray Crystallography', *Biochim. Biophys. Acta*, **1753**, 85–91 (2005).

42. C.H. Trinh, D.P. Smith, A.P. Kalverda, S.E. Phillips, S.E. Radford, 'Crystal Structure of Monomeric Human β-2-Microglobulin Reveals Clues to its Amyloidogenic Properties', *Proc. Natl. Acad. Sci. U S A*, **99**, 9771–9776 (2002).

43. R. Janowski, M. Abrahamson, A. Grubb, M. Jaskolski, 'Domain Swapping in N-Truncated Human Cystatin C', *J. Mol. Biol.*, **341**, 151–160 (2004).

44. M. Kozak, E. Jankowska, R. Janowski, Z. Grzonka, A. Grubb, M. Alvarez Fernandez, M. Abrahamson, M. Jaskolski, 'Expression of a Selenomethionyl Derivative and Preliminary Crystallographic Studies of Human Cystatin C', *Acta Crystallogr. D Biol. Crystallogr.*, **55**, 1939–1942 (1999).

45. R. Janowski, M. Kozak, M. Abrahamson, A. Grubb, M. Jaskolski, '3D Domain-Swapped Human Cystatin C with Amyloidlike Intermolecular β-Sheets', *Proteins*, **61**, 570–578 (2005).

46. C.C. Blake, M.J. Geisow, S.J. Oatley, B. Rerat, C. Rerat, 'Structure of Prealbumin: Secondary, Tertiary and Quaternary Interactions Determined by Fourier Refinement at 1.8 A', *J. Mol. Biol.*, **121**, 339–356 (1978).

47. R.M. Neto-Silva, S. Macedo-Ribeiro, P.J. Pereira, M. Coll, M.J. Saraiva, A.M. Damas, 'X-Ray Crystallographic Studies of two Transthyretin Variants: Further Insights into Amyloidogenesis', *Acta Crystallogr. D. Biol. Crystallogr.*, **61**, 333–339 (2005).

48. K.J. Knaus, M. Morillas, W. Swietnicki, M. Malone, W.K. Surewicz, V.C. Yee, 'Crystal Structure of the Human Prion Protein Reveals a Mechanism for Oligomerization', *Nat. Struct. Biol.*, **8**, 770–774 (2001).

49. R. Nelson, M.R. Sawaya, M. Balbirnie, A.O. Madsen, C. Riekel, R. Grothe, D. Eisenberg, 'Structure of the Cross-β Spine of Amyloid-Like Fibrils', *Nature*, **435**, 773–778 (2005).

50. M.R. Sawaya, S. Sambashivan, R. Nelson, M.I. Ivanova, S.A. Sievers, M.I. Apostol, M.J. Thompson, M. Balbirnie, J.J. Wiltzius, H.T. McFarlane, A.O. Madsen, C. Riekel, D. Eisenberg, 'Atomic Structures of Amyloid Cross-β Spines Reveal Varied Steric Zippers', *Nature*, **447**, 453–457 (2007).

51. K. Takano, S. Endo, A. Mukaiyama, H. Chon, H. Matsumura, Y. Koga, S. Kanaya, 'Structure of Amyloid β Fragments in Aqueous Environments', *FEBS J.*, **273**, 150–158 (2006).

52. E. Morais-de-Sa, P.J. Pereira, M.J. Saraiva, A.M. Damas, 'The Crystal Structure of Transthyretin in Complex with Diethylstilbestrol: A Promising Template for the Design of Amyloid Inhibitors', *J. Biol. Chem.*, **279**, 53483–53490 (2004).

53. K.S. Wun, L.A. Miles, G.A. Crespi, K. Wycherley, D.B. Ascher, K.J. Barnham, R. Cappai, K. Beyreuther, C.L. Masters, M.W. Parker, W.J. McKinstry, 'Crystallization and Preliminary X-Ray Diffraction Analysis of the Fab Fragment of WO2, an Antibody Specific for the Aβ Peptides Associated with Alzheimer's Disease', *Acta Crystallogr. Sect. F Struct. Biol. Cryst. Commun.*, **64**, 438–441 (2008).

54. L.A. Miles, K.S. Wun, G.A. Crespi, M.T. Fodero-Tavoletti, D. Galatis, C.J. Bagley, K. Beyreuther, C.L. Masters, R. Cappai, W.J. McKinstry, K.J. Barnham, M.W. Parker, 'Amyloid-β-Anti-Amyloid-β Complex Structure Reveals an Extended Conformation in the Immunodominant B-cell Epitope', *J. Mol. Biol.*, **377**, 181–192 (2008).

55. B. Akabayov, C.J. Doonan, I.J. Pickering, G.N. George, I. Sagi, 'Using Softer X-Ray Absorption Spectroscopy to Probe Biological Systems', *J. Synchrotron Radiat.*, **12**, 392–401 (2005).

56. V. Streltsov, 'X-Ray Absorption and Diffraction Studies of the Metal Binding Sites in Amyloid β-Peptide', *Eur. Biophys. J.*, **37**, 257–263 (2008).

57. F. Stellato, G. Menestrina, M.D. Serra, C. Potrich, R. Tomazzolli, W. Meyer-Klaucke, S. Morante, 'Metal Binding in Amyloid β-Peptides Shows Intra- and Inter-Peptide Coordination Modes', *Eur. Biophys. J.*, **35**, 340–351 (2006).

58. A. Gaeta, R.C. Hider, 'The Crucial Role of Metal Ions in Neurodegeneration: The Basis for a Promising Therapeutic Strategy', *Br. J. Pharmacol.*, **146**, 1041–1059 (2005).

59. D.G. Smith, R. Cappai, K.J. Barnham, 'The Redox Chemistry of the Alzheimer's Disease Amyloid β Peptide', *Biochim. Biophys. Acta*, **1768**, 1976–1990 (2007).

60. D.R. Brown, K. Qin, J.W. Herms, A. Madlung, J. Manson, R. Strome, P.E. Fraser, T. Kruck, A. von Bohlen, W. Schulz-Schaeffer, A. Giese, D. Westaway, H. Kretzschmar, 'The Cellular Prion Protein Binds Copper In Vivo', *Nature*, **390**, 684–687 (1997).

61. P.C. Pauly, D.A. Harris, 'Copper Stimulates Endocytosis of the Prion Protein', *J. Biol. Chem.*, **273**, 33107–33110 (1998).

62. S. Morante, R. Gonzalez-Iglesias, C. Potrich, C. Meneghini, W. Meyer-Klaucke, G. Menestrina, M. Gasset, 'Inter- and Intra-Octarepeat Cu(II) Site Geometries in the Prion Protein: Implications in Cu(II) Binding Cooperativity and Cu(II)-Mediated Assemblies', *J. Biol. Chem.*, **279**, 11753–11759 (2004).

63. P. del Pino, A. Weiss, U. Bertsch, C. Renner, M. Mentler, K. Grantner, F. Fiorino, W. Meyer-Klaucke, L. Moroder, H.A. Kretzschmar, F.G. Parak, 'The Configuration of the Cu^{2+} Binding Region in Full-Length Human Prion Protein', *Eur. Biophys. J.*, **36**, 239–252 (2007).

64. N.J. Greenfield, 'Using Circular Dichroism Spectra to Estimate Protein Secondary Structure', *Nat. Protoc.*, **1**, 2876–2890 (2006).

65. L. Whitmore, B.A. Wallace, 'Protein Secondary Structure Analyses from Circular Dichroism Spectroscopy: Methods and Reference Databases', *Biopolymers*, **89**, 392–400 (2008).

66. D.M. Walsh, A. Lomakin, G.B. Benedek, M.M. Condron, D.B. Teplow, 'Amyloid β-Protein Fibrillogenesis. Detection of a Protofibrillar Intermediate', *J. Biol. Chem.*, **272**, 22364–22372 (1997).

67. J.D. Harper, C.M. Lieber, P.T. Lansbury, Jr 'Atomic Force Microscopic Imaging of Seeded Fibril Formation and Fibril Branching by the Alzheimer's Disease Amyloid-β Protein', *Chem. Biol.*, **4**, 951–959 (1997).

68. J. Stohr, N. Weinmann, H. Wille, T. Kaimann, L. Nagel-Steger, E. Birkmann, G. Panza, S.B. Prusiner, M. Eigen, D. Riesner, 'Mechanisms of Prion Protein Assembly into Amyloid', *Proc. Natl. Acad. Sci. USA*, **105**, 2409–2414 (2008).

69. M.D. Kirkitadze, M.M. Condron, D.B. Teplow, 'Identification and Characterization of Key Kinetic Intermediates in Amyloid β-Protein Fibrillogenesis', *J. Mol. Biol.*, **312**, 1103–1119 (2001).

70. S. Kumar, S.K. Mohanty, J.B. Udgaonkar, 'Mechanism of Formation of Amyloid Protofibrils of Barstar from Soluble Oligomers: Evidence for Multiple Steps and Lateral Association Coupled to Conformational Conversion', *J. Mol. Biol.*, **367**, 1186–1204 (2007).

71. P. Picotti, G. De Franceschi, E. Frare, B. Spolaore, M. Zambonin, F. Chiti, P.P. de Laureto, A. Fontana, 'Amyloid Fibril Formation and Disaggregation of Fragment 1–29 of Apomyoglobin: Insights into the Effect of pH on Protein Fibrillogenesis', *J. Mol. Biol.*, **367**, 1237–1245 (2007).

72. R. Srinivasan, E.M. Jones, K. Liu, J. Ghiso, R.E. Marchant, M.G. Zagorski, 'pH-Dependent Amyloid and Protofibril Formation by the ABri Peptide of Familial British Dementia', *J. Mol. Biol.*, **333**, 1003–1023 (2003).

73. M.E. Goldberg, A.F. Chaffotte, 'Undistorted Structural Analysis of Soluble Proteins by Attenuated Total Reflectance Infrared Spectroscopy', *Protein Sci.*, **14**, 2781–2792 (2005).

74. B.M. Smith, L. Oswald, S. Franzen, 'Single-Pass Attenuated Total Reflection Fourier Transform Infrared Spectroscopy for the Prediction of Protein Secondary Structure', *Anal. Chem.*, **74**, 3386–3391 (2002).

75. A. Ahmad, V.N. Uversky, D. Hong, A.L. Fink, 'Early Events in the Fibrillation of Monomeric Insulin', *J. Biol. Chem.*, **280**, 42669–42675 (2005).

76. T.R. Jahn, G.A. Tennent, S.E. Radford, 'A Common β-Sheet Architecture Underlies In Vitro and In Vivo β2-Microglobulin Amyloid Fibrils', *J. Biol. Chem.*, **283**, 17279–17286 (2008).

77. H. Hiramatsu, Y. Goto, H. Naiki, T. Kitagawa, 'Core Structure of Amyloid Fibril Proposed from IR-Microscope Linear Dichroism', *J. Am. Chem. Soc.*, **126**, 3008–3009 (2004).

78. H. Hiramatsu, T. Kitagawa, 'FT-IR Approaches on Amyloid Fibril Structure', *Biochim. Biophys. Acta*, **1753**, 100–107 (2005).

79. N. Demirdoven, C.M. Cheatum, H.S. Chung, M. Khalil, J. Knoester, A. Tokmakoff, 'Two-Dimensional Infrared Spectroscopy of Antiparallel β-Sheet Secondary Structure', *J. Am. Chem. Soc.*, **126**, 7981–7990 (2004).

80. Y.S. Kim, L. Liu, P.H. Axelsen, R.M. Hochstrasser, 'Two-Dimensional Infrared Spectra of Isotopically Diluted Amyloid Fibrils from Aβ40', *Proc. Natl. Acad. Sci. USA*, **105**, 7720–7725 (2008).

81. D.B. Strasfeld, Y.L. Ling, S.H. Shim, M.T. Zanni, 'Tracking Fiber Formation in Human Islet Amyloid Polypeptide with Automated 2D-IR Spectroscopy', *J. Am. Chem. Soc.*, **130**, 6698–6699 (2008).

82. M. Sunde, L.C. Serpell, M. Bartlam, P.E. Fraser, M.B. Pepys, C.C. Blake, 'Common Core Structure of Amyloid Fibrils by Synchrotron X-Ray Diffraction', *J. Mol. Biol.*, **273**, 729–739 (1997).

83. H. Inouye, P.E. Fraser, D.A. Kirschner, 'Structure of β-Crystallite Assemblies Formed by Alzheimer β-Amyloid Protein Analogues: Analysis by X-Ray Diffraction', *Biophys. J.*, **64**, 502–519 (1993).

84. J.T. Nguyen, H. Inouye, M.A. Baldwin, R.J. Fletterick, F.E. Cohen, S.B. Prusiner, D.A. Kirschner, 'X-Ray Diffraction of Scrapie Prion Rods and PrP Peptides', *J. Mol. Biol.*, **252**, 412–422 (1995).

85. S. Krueger, D. Ho, A. Tsai, 'Small-Angle Neutron Scattering as a Probe for Protein Aggregation at Many Length Scales', in *Misbehaving Proteins*, eds. R.M. Murphy, A.M. Tsai, Springer, New York, 125–146, 2006.

86. W. Yong, A. Lomakin, M.D. Kirkitadze, D.B. Teplow, S.H. Chen, G.B. Benedek, 'Structure Determination of Micelle-Like Intermediates in Amyloid β-Protein Fibril Assembly by using Small Angle Neutron Scattering', *Proc. Natl. Acad. Sci. USA*, **99**, 150–154 (2002).

87. K. Lu, J. Jacob, P. Thiyagarajan, V.P. Conticello, D.G. Lynn, 'Exploiting Amyloid Fibril Lamination for Nanotube Self-Assembly', *J. Am. Chem. Soc.*, **125**, 6391–6393 (2003).

88. A.C. Hamill, S.C. Wang, C.T. Lee, Jr 'Solution Structure of an Amyloid-Forming Protein During Photoinitiated Hexamer-Dodecamer Transitions Revealed Through Small-Angle Neutron Scattering', *Biochemistry*, **46**, 7694–7705 (2007).

89. R. Virchow, 'Zur Cellulosefrage', *Virchows Arch. Pathol. Anat. Physiol.*, **6**, 416–426 (1854).

90. L.W. Jin, K.A. Claborn, M. Kurimoto, M.A. Geday, I. Maezawa, F. Sohraby, M. Estrada, W. Kaminksy, B. Kahr, 'Imaging Linear Birefringence and Dichroism in Cerebral Amyloid Pathologies', *Proc. Natl. Acad. Sci. USA*, **100**, 15294–15298 (2003).

91. M.T. Elghetany, A. Saleem, 'Methods for Staining Amyloid in Tissues: A Review', *Stain Technol.*, **63**, 201–212 (1988).

92. M.T. Elghetany, A. Saleem, K. Barr, 'The Congo Red Stain Revisited', *Ann. Clin. Lab. Sci.*, **19**, 190–195 (1989).

93. P. Divry, 'Etude Histochimique des Plaques Seniles', *J. Belge. Neurol. Psychiatr.*, **27**, 643–657 (1927).

94. W.E. Klunk, J.W. Pettegrew, D.J. Abraham, 'Quantitative Evaluation of Congo Red Binding to Amyloid-Like Proteins with a β-Pleated Sheet Conformation', *J. Histochem. Cytochem.*, **37**, 1273–1281 (1989).

95. J.H. Cooper, 'Selective Amyloid Staining as a Function of Amyloid Composition and Structure. Histochemical Analysis of the Alkaline Congo Red, Standardized Toluidine Blue, and Iodine Methods', *Lab. Invest.*, **31**, 232–238 (1974).

96. C. Wu, Z. Wang, H. Lei, W. Zhang, Y. Duan, 'Dual Binding Modes of Congo Red to Amyloid Protofibril Surface Observed in Molecular Dynamics Simulations', *J. Am. Chem. Soc.*, **129**, 1225–1232 (2007).

97. D. Brigger, R.J. Muckle, 'Comparison of Sirius Red and Congo Red as Stains for Amyloid in Animal Tissues', *J. Histochem. Cytochem.*, **23**, 84–88 (1975).

98. R. Khurana, C. Coleman, C. Ionescu-Zanetti, S.A. Carter, V. Krishna, R.K. Grover, R. Roy, S. Singh, 'Mechanism of Thioflavin T Binding to Amyloid Fibrils', *J. Struct. Biol.*, **151**, 229–238 (2005).

99. P.S. Vassar, C.F. Culling, 'Fluorescent Stains, with Special Reference to Amyloid and Connective Tissues', *Arch. Pathol.*, **68**, 487–498 (1959).

100. H. LeVine, III 'Quantification of β-Sheet Amyloid Fibril Structures with Thioflavin T', *Methods Enzymol.*, **309**, 274–284 (1999).

101. W.E. Klunk, Y. Wang, G.F. Huang, M.L. Debnath, D.P. Holt, C.A. Mathis, 'Uncharged Thioflavin-T Derivatives Bind to Amyloid- β Protein with High Affinity and Readily Enter The Brain', *Life Sci.*, **69**, 1471–1484 (2001).

102. H. Abe, H. Nakanishi, 'Novel Observation of a Circular Dichroism Band Originating from Amyloid Fibril', *Anal. Sci.*, **19**, 171–173 (2003).

103. T. Ban, Y. Goto, 'Direct Observation of Amyloid Growth Monitored by Total Internal Reflection Fluorescence Microscopy', *Methods Enzymol.*, **413**, 91–102 (2006).

104. M.R. Krebs, E.H. Bromley, A.M. Donald, 'The Binding of Thioflavin-T to Amyloid Fibrils: Localisation and Implications', *J. Struct. Biol.*, **149**, 30–37 (2005).

105. N.M. Kad, N.H. Thomson, D.P. Smith, D.A. Smith, S.E. Radford, 'β2-Microglobulin and its Deamidated Variant, N17D form Amyloid Fibrils with a Range of Morphologies In Vitro', *J. Mol. Biol.*, **313**, 559–571 (2001).

106. H. Yagi, E. Kusaka, K. Hongo, T. Mizobata, Y. Kawata, 'Amyloid Fibril Formation of β-Synuclein is Accelerated by Preformed Amyloid Seeds of other Proteins: Implications for the Mechanism of Transmissible Conformational Diseases', *J. Biol. Chem.*, **280**, 38609–38616 (2005).

107. M. Malisauskas, V. Zamotin, J. Jass, W. Noppe, C.M. Dobson, L.A. Morozova-Roche, 'Amyloid Protofilaments from the Calcium-Binding Protein Equine Lysozyme: Formation of Ring and Linear Structures Depends on pH and Metal Ion Concentration', *J. Mol. Biol.*, **330**, 879–890 (2003).

108. H. LeVine, III 'Thioflavine T Interaction with Synthetic Alzheimer's Disease β-Amyloid Peptides: Detection of Amyloid Aggregation in Solution', *Protein Sci.*, **2**, 404–410 (1993).

109. M.L. Schmidt, K.A. Robinson, V.M. Lee, J.Q. Trojanowski, 'Chemical and Immunological Heterogeneity of Fibrillar Amyloid in Plaques of Alzheimer's Disease and Down's Syndrome Brains Revealed by Confocal Microscopy', *Am. J. Pathol.*, **147**, 503–515 (1995).

110. H. Kowa, T. Sakakura, Y. Matsuura, T. Wakabayashi, D.M. Mann, K. Duff, S. Tsuji, T. Hashimoto, T. Iwatsubo, 'Mostly Separate Distributions of CLAC- Versus Aβ40- or Thioflavin S-Reactivities in Senile Plaques Reveal Two Distinct Subpopulations of β-Amyloid Deposits', *Am. J. Pathol.*, **165**, 273–281 (2004).

111. R.S. Boshuizen, J.P. Langeveld, M. Salmona, A. Williams, R.H. Meloen, J.P. Langedijk, 'An In Vitro Screening Assay Based on Synthetic Prion Protein Peptides for Identification of Fibril-Interfering Compounds', *Anal. Biochem.*, **333**, 372–380 (2004).

112. B. Urbanc, L. Cruz, R. Le, J. Sanders, K.H. Ashe, K. Duff, H.E. Stanley, M.C. Irizarry, B.T. Hyman, 'Neurotoxic Effects of Thioflavin S-Positive Amyloid Deposits in Transgenic Mice and Alzheimer's Disease', *Proc. Natl. Acad. Sci. USA*, **99**, 13990–13995 (2002).

113. F.G. De Felice, J.C. Houzel, J. Garcia-Abreu, P.R. Louzada, Jr, R.C. Afonso, M.N. Meirelles, R. Lent, V.M. Neto, S.T. Ferreira, 'Inhibition of Alzheimer's Disease β-Amyloid Aggregation, Neurotoxicity, and In Vivo Deposition by Nitrophenols: Implications for Alzheimer's Therapy', *FASEB J.*, **15**, 1297–1299 (2001).

114. M.E. McLellan, S.T. Kajdasz, B.T. Hyman, B.J. Bacskai, 'In Vivo Imaging of Reactive Oxygen Species Specifically Associated with Thioflavine S-Positive Amyloid Plaques by Multiphoton Microscopy', *J. Neurosci.*, **23**, 2212–2217 (2003).

115. K. Shoghi-Jadid, G.W. Small, E.D. Agdeppa, V. Kepe, L.M. Ercoli, P. Siddarth, S. Read, N. Satyamurthy, A. Petric, S.C. Huang, J.R. Barrio, 'Localization of Neurofibrillary Tangles and β-Amyloid Plaques in the Brains of Living Patients with Alzheimer Disease', *Am. J. Geriatr. Psychiatry*, **10**, 24–35 (2002).

116. W.E. Klunk, H. Engler, A. Nordberg, Y. Wang, G. Blomqvist, D.P. Holt, M. Bergstrom, I. Savitcheva, G.F. Huang, S. Estrada, B. Ausen, M.L. Debnath, J. Barletta, J.C. Price, J. Sandell, B.J. Lopresti, A. Wall, P. Koivisto, G. Antoni, C.A. Mathis, B. Langstrom, 'Imaging Brain Amyloid in Alzheimer's Disease with Pittsburgh Compound-B', *Ann. Neurol.*, **55**, 306–319 (2004).

117. N.P. Verhoeff, A.A. Wilson, S. Takeshita, L. Trop, D. Hussey, K. Singh, H.F. Kung, M.P. Kung, S. Houle, 'In-Vivo Imaging of Alzheimer Disease β-Amyloid with [^{11}C]SB-13 PET', *Am. J. Geriatr. Psychiatry*, **12**, 584–595 (2004).

118. Y. Kudo, N. Okamura, S. Furumoto, M. Tashiro, K. Furukawa, M. Maruyama, M. Itoh, R. Iwata, K. Yanai, H. Arai, '2-(2-[2-Dimethylaminothiazol-5-yl]ethenyl)-6-(2-[fluoro]ethoxy)Benzoxazole: A Novel PET Agent for In Vivo Detection of Dense Amyloid Plaques in Alzheimer's Disease Patients', *J. Nucl. Med.*, **48**, 553–561 (2007).

119. A. Nordberg, 'Amyloid Imaging in Alzheimer's Disease', *Curr. Opin. Neurol.*, **20**, 398–402 (2007).

120. L. Ye, A. Velasco, G. Fraser, T.G. Beach, L. Sue, T. Osredkar, V. Libri, M.G. Spillantini, M. Goedert, A. Lockhart, 'In Vitro High Affinity β-Synuclein Binding Sites for the Amyloid Imaging Agent PIB are not Matched by Binding to Lewy Bodies in Postmortem Human Brain', *J. Neurochem.*, **105**, 1428–1437 (2008).

121. M.J. Dykstra, L.E. Reuss, *Biological Electron Microscopy : Theory, Techniques, and Troubleshooting*, Kluwer Academic/Plenum Publishers, New York, 2003.

122. H.A. Lashuel, J.S. Wall, 'Molecular Electron Microscopy Approaches to Elucidating the Mechanisms of Protein Fibrillogenesis', *Methods Mol. Biol.*, **299**, 81–101 (2005).

123. W.S. Gosal, S.L. Myers, S.E. Radford, N.H. Thomson, 'Amyloid under the Atomic Force Microscope', *Protein Pept. Lett.*, **13**, 261–270 (2006).

124. A. Steven, D. Belnap, 'Electron Microscopy and Image Processing: An Essential Tool for Structural Analysis of Macromolecules', in *Current Protocols in Protein Science*, ed. G. Taylor, John Wiley & Sons, Inc., New York, 17 12 11–17 12 39, 2007.

125. G. Bitan, M.D. Kirkitadze, A. Lomakin, S.S. Vollers, G.B. Benedek, D.B. Teplow, 'Amyloid β-Protein (Aβ) Assembly: Aβ40 and Aβ42 Oligomerize through Distinct Pathways', *Proc. Natl. Acad. Sci. USA*, **100**, 330–335 (2003).

126. G. Bitan, B. Tarus, S.S. Vollers, H.A. Lashuel, M.M. Condron, J.E. Straub, D.B. Teplow, 'A Molecular Switch in Amyloid Assembly: Met35 and Amyloid β-Protein Oligomerization', *J. Am. Chem. Soc.*, **125**, 15359–15365 (2003).

127. M. Nybo, S.E. Svehag, E. Holm Nielsen, 'An Ultrastructural Study of Amyloid Intermediates in Aβ_{1-42} Fibrillogenesis', *Scand. J. Immunol.*, **49**, 219–223 (1999).

128. A.J. Modler, K. Gast, G. Lutsch, G. Damaschun, 'Assembly of Amyloid Protofibrils Via Critical Oligomers – A Novel Pathway of Amyloid Formation', *J. Mol. Biol.*, **325**, 135–148 (2003).

129. A.E. Roher, M.O. Chaney, Y.M. Kuo, S.D. Webster, W.B. Stine, L.J. Haverkamp, A.S. Woods, R.J. Cotter, J.M. Tuohy, G.A. Krafft, B.S. Bonnell, M.R. Emmerling, 'Morphology and Toxicity of Aβ-(1–42) Dimer Derived from Neuritic and Vascular Amyloid Deposits of Alzheimer's Disease', *J. Biol. Chem.*, **271**, 20631–20635 (1996).

130. M.L. Selenica, X. Wang, L. Ostergaard-Pedersen, A. Westlind-Danielsson, A. Grubb, 'Cystatin C Reduces the In Vitro Formation of Soluble Aβ1-42 Oligomers and Protofibrils', *Scand. J. Clin. Lab. Invest.*, **67**, 179–190 (2007).

131. D.M. Walsh, D.M. Hartley, Y. Kusumoto, Y. Fezoui, M.M. Condron, A. Lomakin, G.B. Benedek, D.J. Selkoe, D.B. Teplow, 'Amyloid β-Protein Fibrillogenesis. Structure and Biological Activity of Protofibrillar Intermediates', *J. Biol. Chem.*, **274**, 25945–25952 (1999).

132. M.R. Nichols, M.A. Moss, D.K. Reed, W.L. Lin, R. Mukhopadhyay, J.H. Hoh, T.L. Rosenberry, 'Growth of β-Amyloid(1–40) Protofibrils by Monomer Elongation and Lateral Association. Characterization of Distinct Products by Light Scattering and Atomic Force Microscopy', *Biochemistry*, **41**, 6115–6127 (2002).

133. I. Kheterpal, H.A. Lashuel, D.M. Hartley, T. Walz, P.T. Lansbury, Jr, R. Wetzel, 'Aβ Protofibrils Possess a Stable Core Structure Resistant to Hydrogen Exchange', *Biochemistry*, **42**, 14092–14098 (2003).

134. R.V. Ward, K.H. Jennings, R. Jepras, W. Neville, D.E. Owen, J. Hawkins, G. Christie, J.B. Davis, A. George, E.H. Karran, D.R. Howlett, 'Fractionation and Characterization of Oligomeric, Protofibrillar and Fibrillar Forms of β-Amyloid Peptide', *Biochem. J.*, **348**(Pt 1), 137–144 (2000).

135. S.J. Wood, B. Maleeff, T. Hart, R. Wetzel, 'Physical, Morphological and Functional Differences between pH 5.8 and 7.4 Aggregates of the Alzheimer's Amyloid Peptide Aβ', *J. Mol. Biol.*, **256**, 870–877 (1996).

136. T. Lührs, C. Ritter, M. Adrian, D. Riek-Loher, B. Bohrmann, H. Döbeli, D. Schubert, R. Riek, '3D Structure of Alzheimer's Amyloid-β(1–42) Fibrils', *Proc. Natl. Acad. Sci. USA*, **102**, 17342–17347 (2005).

137. Bharathi, S.S. Indi, K.S. Rao, 'Copper- and Iron-Induced Differential Fibril Formation in α-Synuclein: TEM Study', *Neurosci. Lett.*, **424**, 78–82 (2007).

138. O. Sumner Makin, L.C. Serpell, 'Structural Characterisation of Islet Amyloid Polypeptide Fibrils', *J. Mol. Biol.*, **335**, 1279–1288 (2004).

139. J.S. Wall, M.N. Simon, B.Y. Lin, S.N. Vinogradov, 'Mass Mapping of Large Globin Complexes by Scanning Transmission Electron Microscopy', *Methods Enzymol.*, **436**, 487–501 (2008).

140. C. Goldsbury, P. Frey, V. Olivieri, U. Aebi, S.A. Muller, 'Multiple Assembly Pathways Underlie Amyloid-β Fibril Polymorphisms', *J. Mol. Biol.*, **352**, 282–298 (2005).

141. C.S. Goldsbury, S. Wirtz, S.A. Muller, S. Sunderji, P. Wicki, U. Aebi, P. Frey, 'Studies on the In Vitro Assembly of Aβ 1–40: Implications for the Search for Aβ Fibril Formation Inhibitors', *J. Struct. Biol.*, **130**, 217–231 (2000).

142. A.T. Petkova, R.D. Leapman, Z. Guo, W.M. Yau, M.P. Mattson, R. Tycko, 'Self-Propagating, Molecular-Level Polymorphism in Alzheimer's β-Amyloid Fibrils', *Science*, **307**, 262–265 (2005).

143. P.K. Hansma, V.B. Elings, O. Marti, C.E. Bracker, 'Scanning Tunneling Microscopy and Atomic Force Microscopy: Application to Biology and Technology', *Science*, **242**, 209–216 (1988).

144. A.P. Shivji, F. Brown, M.C. Davies, K.H. Jennings, C.J. Roberts, S. Tendler, M.J. Wilkinson, P.M. Williams, 'Scanning Tunnelling Microscopy Studies of β-Amyloid Fibril Structure and Assembly', *FEBS Lett.*, **371**, 25–28 (1995).

145. Z. Wang, C. Zhou, C. Wang, L. Wan, X. Fang, C. Bai, 'AFM and STM Study of β-Amyloid Aggregation on Graphite', *Ultramicroscopy*, **97**, 73–79 (2003).

146. D. Losic, L.L. Martin, A. Mechler, M.I. Aguilar, D.H. Small, 'High Resolution Scanning Tunnelling Microscopy of the β-Amyloid Protein (Aβ 1–40) of Alzheimer's Disease Suggests a Novel Mechanism of Oligomer Assembly', *J. Struct. Biol.*, **155**, 104–110 (2006).

147. C. Goldsbury, J. Green, 'Time-Lapse Atomic Force Microscopy in the Characterization of Amyloid-Like Fibril Assembly and Oligomeric Intermediates', *Methods Mol. Biol.*, **299**, 103–128 (2005).

148. H.K. Blackley, G.H. Sanders, M.C. Davies, C.J. Roberts, S.J. Tendler, M.J. Wilkinson, 'In-Situ Atomic Force Microscopy Study of β-Amyloid Fibrillization', *J. Mol. Biol.*, **298**, 833–840 (2000).

149. J.H. Lee, G. Bhak, S.G. Lee, S.R. Paik, 'Instantaneous Amyloid Fibril Formation of β-Synuclein from the Oligomeric Granular Structures in the Presence of Hexane', *Biophys. J.*, **95**, L16–L18 (2008).

150. C. Ionescu-Zanetti, R. Khurana, J.R. Gillespie, J.S. Petrick, L.C. Trabachino, L.J. Minert, S.A. Carter, A.L. Fink, 'Monitoring the Assembly of Ig Light-Chain Amyloid Fibrils by Atomic Force Microscopy', *Proc. Natl. Acad. Sci. USA*, **96**, 13175–13179 (1999).

151. S. Kunze, K. Lemke, J. Metze, G. Bloukas, K. Kotta, C.H. Panagiotidis, T. Sklaviadis, W. Bodemer, 'Atomic Force Microscopy to Characterize the Molecular Size of Prion Protein', *J. Microsc.*, **230**, 224–232 (2008).

152. I.A. Mastrangelo, M. Ahmed, T. Sato, W. Liu, C. Wang, P. Hough, S.O. Smith, 'High-Resolution Atomic Force Microscopy of Soluble Aβ42 Oligomers', *J. Mol. Biol.*, **358**, 106–119 (2006).

153. E. Zavoisky, 'Spin-Magnetic Resonance in Paramagnetics', *J. Phys. USSR*, **9**, 211–216 (1945).

154. J.F. Boas, S.C. Drew, C.C. Curtain, 'Applications of Electron Paramagnetic Resonance to Studies of Neurological Disease', *Eur. Biophys. J.*, **37**, 281–294 (2008).

155. D.A. Butterfield, 'Amyloid β-Peptide [1–42]-Associated Free Radical-Induced Oxidative Stress and Neurodegeneration in Alzheimer's Disease Brain: Mechanisms and Consequences', *Curr. Med. Chem.*, **10**, 2651–2659 (2003).

156. K. Murakami, K. Irie, H. Ohigashi, H. Hara, M. Nagao, T. Shimizu, T. Shirasawa, 'Formation and Stabilization Model of the 42-mer Aβ Radical: Implications for the Long-Lasting Oxidative Stress in Alzheimer's disease', *J. Am. Chem. Soc.*, **127**, 15168–15174 (2005).

157. B.J. Tabner, S. Turnbull, O. El-Agnaf, D. Allsop, 'Production of Reactive Oxygen Species from Aggregating Proteins Implicated in Alzheimer's Disease, Parkinson's Disease and other Neurodegenerative Diseases', *Curr. Top. Med. Chem.*, **1**, 507–517 (2001).

158. M. Török, S. Milton, R. Kayed, P. Wu, T. McIntire, C.G. Glabe, R. Langen, 'Structural and Dynamic Features of Alzheimer's Aβ Peptide in Amyloid Fibrils Studied by Site-Directed Spin Labeling', *J. Biol. Chem.*, **277**, 40810–40815 (2002).

159. K. Murakami, H. Hara, Y. Masuda, H. Ohigashi, K. Irie, 'Distance Measurement between Tyr10 and Met35 in Amyloid β by Site-Directed Spin-Labeling ESR Spectroscopy: Implications for the Stronger Neurotoxicity of Aβ42 than Aβ40', *ChemBioChem*, **8**, 2308–2314 (2007).

160. S.A. Jayasinghe, R. Langen, 'Identifying Structural Features of Fibrillar Islet Amyloid Polypeptide using Site-Directed Spin Labeling', *J. Biol. Chem.*, **279**, 48420–48425 (2004).

161. M. Chen, M. Margittai, J. Chen, R. Langen, 'Investigation of α-Synuclein Fibril Structure by Site-Directed Spin Labeling', *J. Biol. Chem.*, **282**, 24970–24979 (2007).

162. T.E. Wales, J.R. Engen, 'Hydrogen Exchange Mass Spectrometry for the Analysis of Protein Dynamics', *Mass Spectrom. Rev.*, **25**, 158–170 (2006).

163. M. Hoshino, H. Katou, K. Yamaguchi, Y. Goto, 'Dimethylsulfoxide-Quenched Hydrogen/Deuterium Exchange Method to Study Amyloid Fibril Structure', *Biochim. Biophys. Acta*, **1768**, 1886–1899 (2007).

164. S. Cavadini, A. Abraham, G. Bodenhausen, 'Coherence Transfer between Spy Nuclei and Nitrogen-14 In Solids', *J. Magn. Reson.*, **190**, 160–164 (2008).

165. N.A. Whittemore, R. Mishra, I. Kheterpal, A.D. Williams, R. Wetzel, E.H. Serpersu, 'Hydrogen-Deuterium (H/D) Exchange Mapping of Aβ_{1-40} Amyloid Fibril Secondary Structure using Nuclear Magnetic Resonance Spectroscopy', *Biochemistry*, **44**, 4434–4441 (2005).

166. Y. Tsutsui, P.L. Wintrode, 'Hydrogen/Deuterium Exchange–Mass Spectrometry: A Powerful Tool for Probing Protein Structure, Dynamics and Interactions', *Curr. Med. Chem.*, **14**, 2344–2358 (2007).

167. I. Kheterpal, M. Chen, K.D. Cook, R. Wetzel, 'Structural Differences in Aβ Amyloid Protofibrils and Fibrils Mapped by Hydrogen Exchange–Mass Spectrometry with On-Line Proteolytic Fragmentation', *J. Mol. Biol.*, **361**, 785–795 (2006).

168. N. Carulla, G.L. Caddy, D.R. Hall, J. Zurdo, M. Gairi, M. Feliz, E. Giralt, C.V. Robinson, C.M. Dobson, 'Molecular Recycling within Amyloid Fibrils', *Nature*, **436**, 554–558 (2005).

169. I. Kheterpal, A. Williams, C. Murphy, B. Bledsoe, R. Wetzel, 'Structural Features of the Aβ Amyloid Fibril

Elucidated by Limited Proteolysis', *Biochemistry*, **40**, 11757–11767 (2001).

170. N.D. Lazo, M.A. Grant, M.C. Condron, A.C. Rigby, D.B. Teplow, 'On the Nucleation of Amyloid β-Protein Monomer Folding', *Protein Sci.*, **14**, 1581–1596 (2005).

171. S.L. Myers, N.H. Thomson, S.E. Radford, A.E. Ashcroft, 'Investigating the Structural Properties of Amyloid-Like Fibrils Formed In Vitro From β2-Microglobulin using Limited Proteolysis and Electrospray Ionisation Mass Spectrometry', *Rapid Commun. Mass Spectrom.*, **20**, 1628–1636 (2006).

172. L.A. Munishkina, A.L. Fink, 'Fluorescence as a Method to Reveal Structures and Membrane-Interactions of Amyloidogenic Proteins', *Biochim. Biophys. Acta*, **1768**, 1862–1885 (2007).

173. S.K. Maji, J.J. Amsden, K.J. Rothschild, M.M. Condron, D.B. Teplow, 'Conformational Dynamics of Amyloid β-Protein Assembly Probed using Intrinsic Fluorescence', *Biochemistry*, **44**, 13365–13376 (2005).

174. V. Tõugu, A. Karafin, P. Palumaa, 'Binding of Zinc(II) and Copper(II) to the Full-Length Alzheimer's Amyloid-β Peptide', *J. Neurochem.*, **104**, 1249–1259 (2008).

175. S.B. Padrick, A.D. Miranker, 'Islet Amyloid Polypeptide: Identification of Long-Range Contacts and Local Order on the Fibrillogenesis Pathway', *J. Mol. Biol.*, **308**, 783–794 (2001).

176. L. Stryer, 'Fluorescence Energy Transfer as a Spectroscopic Ruler', *Annu. Rev. Biochem.*, **47**, 819–846 (1978).

177. W. Garzon-Rodriguez, M. Sepulveda-Becerra, S. Milton, C.G. Glabe, 'Soluble Amyloid Aβ (1–40) Exists as a Stable Dimer at Low Concentrations', *J. Biol. Chem.*, **272**, 21037–21044 (1997).

178. J. Kim, M. Lee, 'Observation of Multi-Step Conformation Switching in β-Amyloid Peptide Aggregation by Fluorescence Resonance Energy Transfer', *Biochem. Biophys. Res. Commun.*, **316**, 393–397 (2004).

179. J.C. Lee, R. Langen, P.A. Hummel, H.B. Gray, J.R. Winkler, 'α-Synuclein Structures from Fluorescence Energy-Transfer Kinetics: Implications for the Role of the Protein in Parkinson's Disease', *Proc. Natl. Acad. Sci. USA*, **101**, 16466–16471 (2004).

180. S. Mukhopadhyay, R. Krishnan, E.A. Lemke, S. Lindquist, A.A. Deniz, 'A Natively Unfolded Yeast Prion Monomer Adopts an Ensemble of Collapsed and Rapidly Fluctuating Structures', *Proc. Natl. Acad. Sci. USA*, **104**, 2649–2654 (2007).

181. W. Kim, M.H. Hecht, 'Generic Hydrophobic Residues are Sufficient to Promote Aggregation of the Alzheimer's Aβ42 Peptide', *Proc. Natl. Acad. Sci. USA*, **103**, 15824–15829 (2006).

182. W. Kim, Y. Kim, J. Min, D.J. Kim, Y.T. Chang, M.H. Hecht, 'A High-Throughput Screen for Compounds that Inhibit Aggregation of the Alzheimer's Peptide', *ACS Chem. Biol.*, **1**, 461–469 (2006).

183. T. Pederson, 'Turning a PAGE: The Overnight Sensation of SDS-Polyacrylamide Gel Electrophoresis', *FASEB J.*, **22**, 949–953 (2008).

184. P.G. Righetti, 'Bioanalysis: Its Past, Present, and Some Future', *Electrophoresis*, **25**, 2111–2127 (2004).

185. K.L. Gudiksen, I. Gitlin, G.M. Whitesides, 'Differentiation of Proteins Based on Characteristic Patterns of Association and Denaturation in Solutions of SDS', *Proc. Natl. Acad. Sci. USA*, **103**, 7968–7972 (2006).

186. K.W. Leffers, J. Schell, K. Jansen, R. Lucassen, T. Kaimann, L. Nagel-Steger, J. Tatzelt, D. Riesner, 'The Structural Transition of the Prion Protein into its Pathogenic Conformation is Induced by Unmasking Hydrophobic Sites', *J. Mol. Biol.*, **344**, 839–853 (2004).

187. J.K. Kawooya, T.L. Emmons, P.A. Gonzalez-DeWhitt, M.C. Camp, S.C. D'Andrea, 'Electrophoretic Mobility of Alzheimer's Amyloid-β Peptides in Urea-Sodium Dodecyl Sulfate-Polyacrylamide Gel Electrophoresis', *Anal. Biochem.*, **323**, 103–113 (2003).

188. R. Montserret, M.J. McLeish, A. Bockmann, C. Geourjon, F. Penin, 'Involvement of Electrostatic Interactions in the Mechanism of Peptide Folding Induced by Sodium Dodecyl Sulfate Binding', *Biochemistry*, **39**, 8362–8373 (2000).

189. S. Yamamoto, K. Hasegawa, I. Yamaguchi, S. Tsutsumi, J. Kardos, Y. Goto, F. Gejyo, H. Naiki, 'Low Concentrations of Sodium Dodecyl Sulfate Induce the Extension of β_2-Microglobulin-Related Amyloid Fibrils at a Neutral pH', *Biochemistry*, **43**, 11075–11082 (2004).

190. V. Rangachari, B.D. Moore, D.K. Reed, L.K. Sonoda, A.W. Bridges, E. Conboy, D. Hartigan, T.L. Rosenberry, 'Amyloid-β(1–42) Rapidly forms Protofibrils and Oligomers by Distinct Pathways in Low Concentrations of Sodium Dodecylsulfate', *Biochemistry*, **46**, 12451–12462 (2007).

191. V. Rangachari, D.K. Reed, B.D. Moore, T.L. Rosenberry, 'Secondary Structure and Interfacial Aggregation of Amyloid-β(1–40) on Sodium Dodecyl Sulfate Micelles', *Biochemistry*, **45**, 8639–8648 (2006).

192. N. Piening, P. Weber, T. Hogen, M. Beekes, H. Kretzschmar, A. Giese, 'Photo-Induced Crosslinking of Prion Protein Oligomers and Prions', *Amyloid*, **13**, 67–77 (2006).

193. S. Barghorn, V. Nimmrich, A. Striebinger, C. Krantz, P. Keller, B. Janson, M. Bahr, M. Schmidt, R.S. Bitner, J. Harlan, E. Barlow, U. Ebert, H. Hillen, 'Globular Amyloid β-Peptide$_{1-42}$ Oligomer–A Homogenous and Stable Neuropathological Protein in Alzheimer's Disease', *J. Neurochem.*, **95**, 834–847 (2005).

194. G. Bitan, E.A. Fradinger, S.M. Spring, D.B. Teplow, 'Neurotoxic Protein Oligomers–what you see is not always what you get', *Amyloid*, **12**, 88–95 (2005).

195. C.E. Moussa, C. Wersinger, M. Rusnak, Y. Tomita, A. Sidhu, 'Abnormal Migration of Human Wild-Type α-Synuclein upon Gel Electrophoresis', *Neurosci. Lett.*, **371**, 239–243 (2004).

196. H. Mori, K. Takio, M. Ogawara, D.J. Selkoe, 'Mass Spectrometry of Purified Amyloid β Protein in Alzheimer's Disease', *J. Biol. Chem.*, **267**, 17082–17086 (1992).

197. R.W. Hepler, K.M. Grimm, D.D. Nahas, R. Breese, E.C. Dodson, P. Acton, P.M. Keller, M. Yeager, H. Wang, P. Shughrue, G. Kinney, J.G. Joyce, 'Solution State Characterization of Amyloid β -Derived Diffusible Ligands', *Biochemistry*, **45**, 15157–15167 (2006).

198. G. Bitan, 'Structural Study of Metastable Amyloidogenic Protein Oligomers by Photo-Induced Cross-Linking of Unmodified Proteins', *Methods Enzymol.*, **413**, 217–236 (2006).

199. D.A. Fancy, T. Kodadek, 'Chemistry for the Analysis of Protein-Protein Interactions: Rapid and Efficient Cross-Linking Triggered by Long Wavelength Light', *Proc. Natl. Acad. Sci. USA*, **96**, 6020–6024 (1999).

200. R. Kluger, A. Alagic, 'Chemical Cross-Linking and Protein-Protein Interactions-a Review with Illustrative Protocols', *Bioorg. Chem.*, **32**, 451–472 (2004).

201. G. Bitan, D.B. Teplow, 'Rapid Photochemical Cross-Linking-a New Tool for Studies of Metastable, Amyloidogenic Protein Assemblies', *Acc. Chem. Res.*, **37**, 357–364 (2004).

202. H.T. Li, X.J. Lin, Y.Y. Xie, H.Y. Hu, 'The Early Events of α-Synuclein Oligomerization Revealed by Photo-Induced Cross-Linking', *Protein Pept. Lett.*, **13**, 385–390 (2006).

203. T.M. Squires, J.F. Brady, 'A Simple Paradigm for Active and Nonlinear Microrheology', *Phys. Fluids*, **17**, 073101 (2005).

204. A. Westlind-Danielsson, G. Arnerup, 'Spontaneous In Vitro Formation of Supramolecular β-Amyloid Structures, "βamy Balls", by β-Amyloid 1–40 Peptide', *Biochemistry*, **40**, 14736–14743 (2001).

205. H.A. Lashuel, D.M. Hartley, B.M. Petre, J.S. Wall, M.N. Simon, T. Walz, P.T. Lansbury, Jr, 'Mixtures of Wild-Type and a Pathogenic (E22G) Form of Aβ40 In Vitro Accumulate Protofibrils, Including Amyloid Pores', *J. Mol. Biol.*, **332**, 795–808 (2003).

206. G. Bitan, A. Lomakin, D.B. Teplow, 'Amyloid β-Protein Oligomerization: Prenucleation Interactions Revealed by Photo-Induced Cross-Linking of Unmodified Proteins', *J. Biol. Chem.*, **276**, 35176–35184 (2001).

207. L. Banci, I. Bertini, M. Boca, S. Girotto, M. Martinelli, J.S. Valentine, M. Vieru, 'SOD1 and Amyotrophic Lateral Sclerosis: Mutations and Oligomerization', *PLoS ONE*, **3**, e1677 (2008).

208. G. Bitan, D.B. Teplow, 'Preparation of Aggregate-Free, Low Molecular Weight Amyloid-β for Assembly and Toxicity Assays', *Methods Mol. Biol.*, **299**, 3–9 (2005).

209. H.A. Lashuel, D.M. Hartley, D. Balakhaneh, A. Aggarwal, S. Teichberg, D.J. Callaway, 'New Class of Inhibitors of Amyloid-β Fibril Formation. Implications for the Mechanism of Pathogenesis in Alzheimer's Disease', *J. Biol. Chem.*, **277**, 42881–42890 (2002).

210. H.A. Lashuel, Z. Lai, J.W. Kelly, 'Characterization of the Transthyretin Acid Denaturation Pathways by Analytical Ultracentrifugation: Implications for Wild-Type, V30M, and L55P Amyloid Fibril Formation', *Biochemistry*, **37**, 17851–17864 (1998).

211. Y.F. Mok, G.J. Howlett, 'Sedimentation Velocity Analysis of Amyloid Oligomers and Fibrils', *Methods Enzymol.*, **413**, 199–217 (2006).

212. T.H. Huang, D.S. Yang, N.P. Plaskos, S. Go, C.M. Yip, P.E. Fraser, A. Chakrabartty, 'Structural Studies of Soluble Oligomers of the Alzheimer β -Amyloid Peptide', *J. Mol. Biol.*, **297**, 73–87 (2000).

213. J.S. Philo, 'Is any Measurement Method Optimal for all Aggregate Sizes and Types?' *AAPS J.*, **8**, E564–E571 (2006).

214. A. Einstein, 'On the Motion of Small Particles Suspended in Liquids at Rest Required by the Molecular-Kinetic Theory of Heat', *Ann. Phys.*, **17**, 549–560 (1905).

215. W. Sutherland, 'A Dynamical Theory of Diffusion for Non-Electrolytes and the Molecular Mass of Albumin', *Philos. Mag.*, **9**, 781–785 (1905).

216. A. Lomakin, G.B. Benedek, D.B. Teplow, 'Monitoring Protein Assembly using Quasielastic Light Scattering Spectroscopy', *Methods Enzymol.*, **309**, 429–459 (1999).

217. P.J. Wyatt, 'Light-Scattering and the Absolute Characterization of Macromolecules', *Anal. Chim. Acta*, **272**, 1–40 (1993).

218. A. Oliva, M. Llabres, J.B. Farina, 'Applications of Multi-Angle Laser Light-Scattering Detection in the Analysis of Peptides and Proteins', *Curr. Drug Discov. Technol.*, **1**, 229–242 (2004).

219. M. Mauro, E.F. Craparo, A. Podesta, D. Bulone, R. Carrotta, V. Martorana, G. Tiana, P.L. San Biagio, 'Kinetics of Different Processes in Human Insulin Amyloid Formation', *J. Mol. Biol.*, **366**, 258–274 (2007).

220. C. Avidan-Shpalter, E. Gazit, 'The Early Stages of Amyloid Formation: Biophysical and Structural Characterization of Human Calcitonin Pre-Fibrillar Assemblies', *Amyloid*, **13**, 216–225 (2006).

221. A. Lomakin, D.B. Teplow, 'Quasielastic Light Scattering Study of Amyloid β-Protein Fibril Formation', *Protein Pept. Lett.*, **13**, 247–254 (2006).

222. A. Lomakin, D.B. Teplow, G.B. Benedek, 'Quasielastic Light Scattering for Protein Assembly Studies', *Methods Mol. Biol.*, **299**, 153–174 (2005).

223. S.J. Tomski, R.M. Murphy, 'Kinetics of Aggregation of Synthetic β-Amyloid Peptide', *Arch. Biochem. Biophys.*, **294**, 630–638 (1992).

224. C.L. Shen, G.L. Scott, F. Merchant, R.M. Murphy, 'Light Scattering Analysis of Fibril Growth from the Amino-Terminal Fragment $\beta(1-28)$ of β-Amyloid Peptide', *Biophys. J.*, **65**, 2383–2395 (1993).

225. A. Lomakin, D.S. Chung, G.B. Benedek, D.A. Kirschner, D.B. Teplow, 'On the Nucleation and Growth of Amyloid β-Protein Fibrils: Detection of Nuclei and Quantitation of Rate Constants', *Proc. Natl. Acad. Sci. USA*, **93**, 1125–1129 (1996).

226. R.M. Murphy, M.M. Pallitto, 'Probing the Kinetics of β-Amyloid Self-Association', *J. Struct. Biol.*, **130**, 109–122 (2000).

227. L. Redecke, M. von Bergen, J. Clos, P.V. Konarev, D.I. Svergun, U.E. Fittschen, J.A. Broekaert, O. Bruns, D. Georgieva, E. Mandelkow, N. Genov, C. Betzel, 'Structural Characterization of β-Sheeted Oligomers Formed on the Pathway of Oxidative Prion Protein Aggregation In Vitro', *J. Struct. Biol.*, **157**, 308–320 (2007).

228. A.B. Kanu, P. Dwivedi, M. Tam, L. Matz, H.H. Hill, Jr 'Ion Mobility-Mass Spectrometry', *J. Mass Spectrom.*, **43**, 1–22 (2008).

229. K. Tang, F. Li, A.A. Shvartsburg, E.F. Strittmatter, R.D. Smith, 'Two-Dimensional Gas-Phase Separations Coupled to Mass Spectrometry for Analysis of Complex Mixtures', *Anal. Chem.*, **77**, 6381–6388 (2005).

230. T. Wyttenbach, M.T. Bowers, 'Gas-Phase Conformations: The Ion Mobility/Ion Chromatography Method', *Top. Curr. Chem.*, **225**, 207–232 (2003).

231. S.L. Bernstein, T. Wyttenbach, A. Baumketner, J.E. Shea, G. Bitan, D.B. Teplow, M.T. Bowers, 'Amyloid β-Protein: Monomer Structure and Early Aggregation States of Aβ42 and its Pro19 Alloform', *J. Am. Chem. Soc.*, **127**, 2075–2084 (2005).

232. S.L. Bernstein, D. Liu, T. Wyttenbach, M.T. Bowers, J.C. Lee, H.B. Gray, J.R. Winkler, 'α-Synuclein: Stable Compact and Extended Monomeric Structures and pH Dependence of Dimer Formation', *J. Am. Soc. Mass Spectrom.*, **15**, 1435–1443 (2004).

233. A.J. Borysik, P. Read, D.R. Little, R.H. Bateman, S.E. Radford, A.E. Ashcroft, 'Separation of β2−Microglobulin Conformers by High-Field Asymmetric Waveform Ion Mobility Spectrometry (FAIMS) Coupled to Electrospray Ionisation Mass Spectrometry', *Rapid Commun. Mass Spectrom.*, **18**, 2229–2234 (2004).

234. A.A. Shvartsburg, F. Li, K. Tang, R.D. Smith, 'Characterizing the Structures and Folding of Free Proteins using 2-D Gas-Phase Separations: Observation of Multiple Unfolded Conformers', *Anal. Chem.*, **78**, 3304–3315 (2006).